FINAL TECHNICAL REPORT

Confirming and Extending the Holocene Event History at Hog Lake, San Jacinto fault: Testing San Andreas - San Jacinto Fault interactions

U.S.G.S GRANT NO. 08HQGR0063

Thomas Rockwell, P.I.

Gordon Seitz, Co-P.I.

J. Barrett Salisbury

Michael Buga

Geological Sciences
San Diego State University
San Diego, CA 92182
Trockwel@geology.sdsu.edu

Table of Contents

Cover Page	1
Table of Contents	ii
Summary	3
Project Overview	3
Rupture Distribution Mapping	5
The South Fork Wilderness Site	9
The Clark Lake Paleoseismic Site	11
Conclusions	13
References Cited	14

Summary

The primary foci of this project was to confirm the cluster of events between about AD 1000 and 1400, determined for the central Clark strand of the San Jacinto fault at Hog Lake, and if possible, to extend the record of surface ruptures to as much as 5 ka, and then to compare the record of ruptures from the central San Jacinto fault to that of the San Andreas fault. Hog Lake is located on the Ramona Indian reservation near Anza, and during the initial phase of funding, leadership in the reservation changed. This resulted in a series of requests, including expensive biological analyses of the site, which ultimately resulted in our inability to continue working at the site. To fulfill the goals of the project, we undertook four tasks that greatly expanded our knowledge base on the rupture history of the central San Jacinto fault zone. These included determination of the amount of displacement in the past three ruptures for the Clark fault by completing mapping of the rupture distribution from Anza northwest to Hemet; excavation of a trench at a new site a few kilometers northwest from Hog Lake to test for the 1918 and 1800 surface ruptures; and initiation of excavations at a new site in Clark Lake to test for similarity of rupture histories to that at Hog Lake. The new trenches are all located in Wilderness areas, which led to a long permitting process, but have yielded excellent data on the rupture history both to the north and south of Hog Lake. From these data, we are now in a position to publish a sequence of papers that will greatly increase the present state of knowledge of the "western branch" of the San Andreas fault system in southern California.

Project Overview

The Clark fault is the longest, continuous, and straightest strand of the San Jacinto fault zone, extending nearly 100 km from the San Filipe Hills in the western Salton Trough northwestward to the Hemet Valley area (Figure 1). The Casa Loma fault continues the Clark strand to the releasing step-over at Mystic Lake in the San Jacinto Valley, where slip steps to the Claremont fault and continues to the its juncture with the San Andreas fault. Mystic Lake itself is another new paleoseismic site that is being developed with NEHRP funding (Onderdonk et al., 2010). Together, the Clark and Casa Loma faults comprise a straight, continuous zone that extends for about 125 km, and if ruptured in a single event, may produce earthquakes that measure in the mid-M7 range.

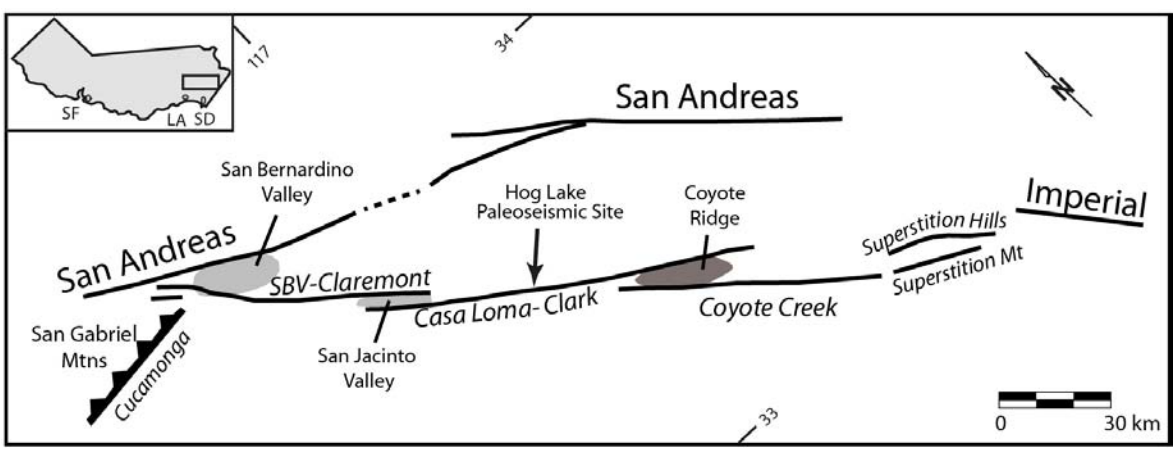

Figure 1. *Generalized map of the San Jacinto and southern San Andreas Fault zones indicating the large scale segmentation of the fault zones (modified from Sanders and Magistrale, 1997).*

Hog Lake is a small ephemeral basin along the central portion of the Clark fault, produced by a ~100m right step in the fault (Figure 2). The site is near the northwestern end of the Anza Seismicity Gap, an approximately 20 km section of fault that exhibits a suppressed level of microseismicity, and along which seismicity extends to about 20 km depth. It has therefore been attributed as having the possibility of the largest displacement per event along the length of the San Jacinto fault zone.

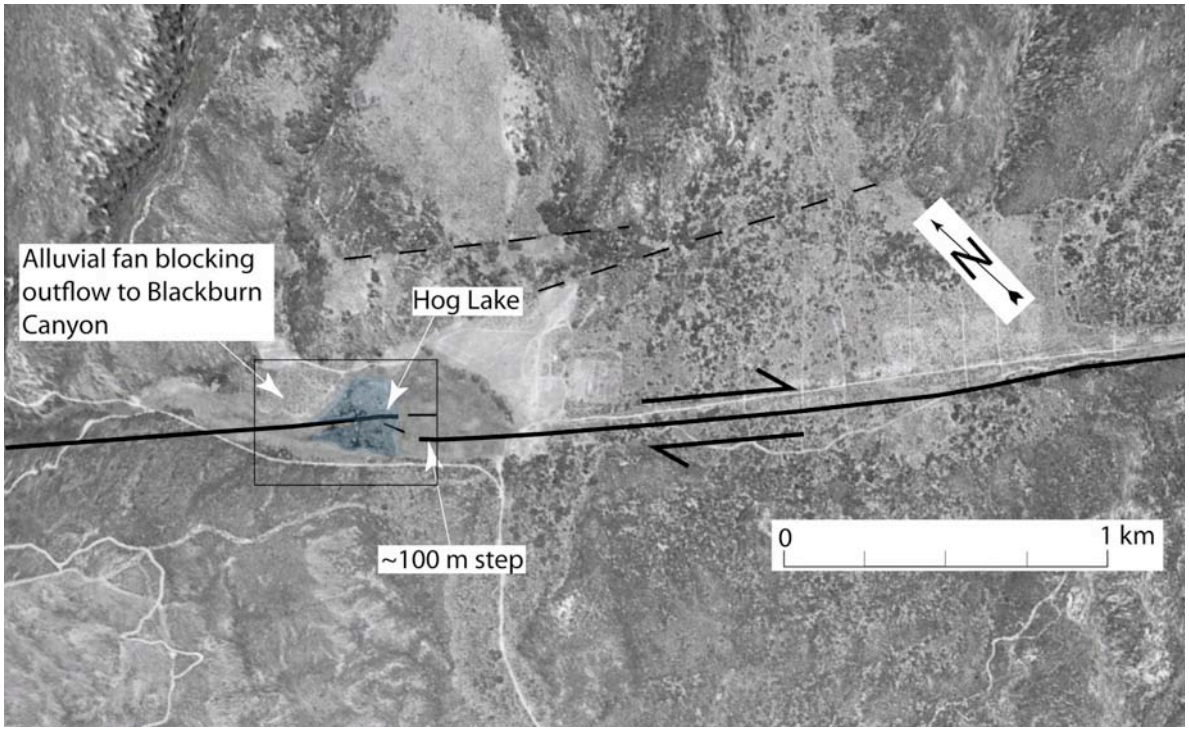

Figure 2. *The Hog Lake trench site northwest of Anza on the Ramona Indian Reservation.*

Paleoseismic studies were begun at Hog Lake in the mid-1980's (Klinger and Rockwell, 1987), and continued with NEHRP support in 2002 and 2004 (Rockwell et al., 2003, 2006). In these studies, progressively deeper trenches (Figure 3) exposed evidence for up to 18 surface-rupturing events in the past 4,000 years (Figure 4), yielding an average recurrence interval of about 210 years. Questions remain about the completeness of the record, as well as whether some interpreted events may represent evidence for two events. Hence, additional studies were planned to address these uncertainties.

Simultaneously, paleoseismic studies were being carried out on the Coyote Creek and Superstition Mountains strands of the fault zone (Rockwell et al, 2000; Ragona et al., 2001; Verdugo et al., 2005; Rockwell et al., 2005), with the intent of developing the complete rupture history of the southernmost elements of the San Jacinto fault zone for the past 1-2 ka. Part of this work includes mapping of the small geomorphic offsets along the various fault elements to establish slip in the most recent few events (Middleton, 2006; Salisbury et al., 2011 in review; Pandey and Rockwell, in progress). Most recently, new studies have been undertaken at Clark Lake on the southern Clark fault, and at Mystic Lake on the Claremont fault, which when completed, will add to the richness of the existing set of data. Most of the earlier studies have been submitted for publication or are in various stages of completion. The Hog Lake dataset was

awaiting final resolution of the status of additional trenching, and now that that has been resolved (negatively), we are moving forward with final publication on the paleoseismic work completed at that site to date.

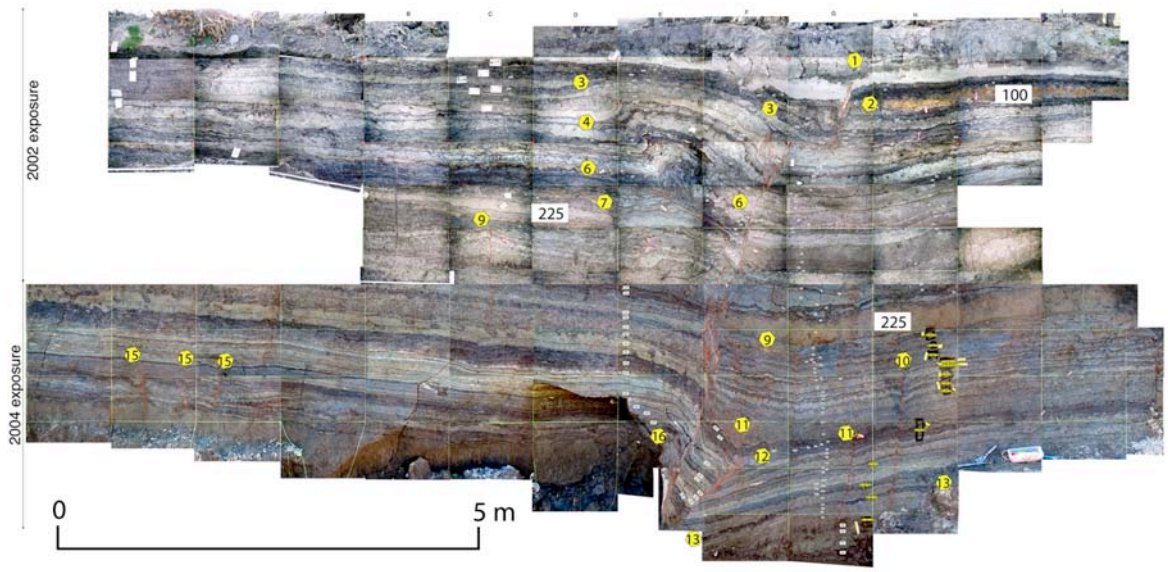

Figure 3. *The deepT2N exposure at Hog Lake.*

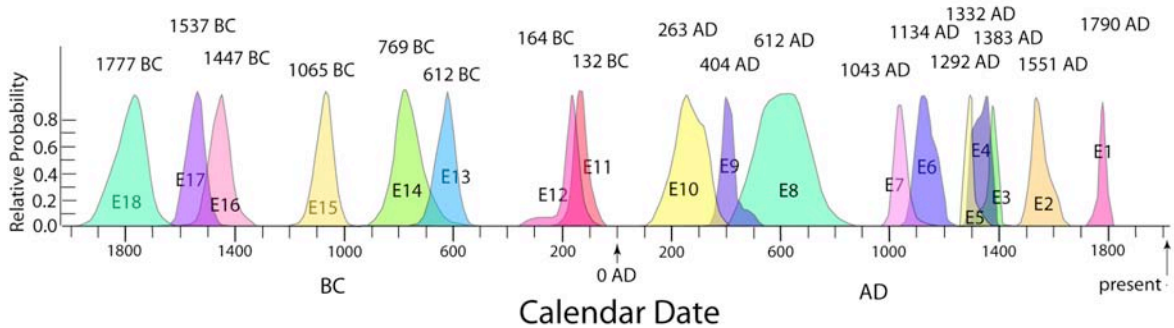

Figure 4. *Ages of surface ruptures recognized at Hog Lake.*

In the following sections, the new works completed for this project are presented by area and topic. We begin with the completion of mapping of small geomorphic offsets, as this project led to the recognition of the (probable) 1918 rupture and associated offsets. We then present new paleoseismic data from a trench along the 1918 rupture in the South Fork Wilderness Area located a few kms northwest from Hog Lake (Figure 5). We then present the initial work begun at Clark Lake (Figure 5), which we will use to confirm and compare to the Hog Lake record.

Rupture Distribution Mapping

Small geomorphic offsets along the southern half of the Clark fault were studied as part of an MS thesis by T.J. Middleton, completed in 2006. This work was continued as the MS thesis project of J.B. Salisbury, and part of the funding for his project was derived from the Hog Lake funding to complete the mapping and see the manuscript written and submitted for

publication. In these works, one of the main foci were to understand distribution of slip in past earthquakes, which relates to both the size of the events as well as understanding whether the Clark strand of the fault zone is segmented and ruptures in smaller events, or whether the entire strand is likely to rupture in a single event. The B4 LiDAR dataset were used for both studies, and all offsets were mapped and measured in the field, as well as by remotely-sensed data.

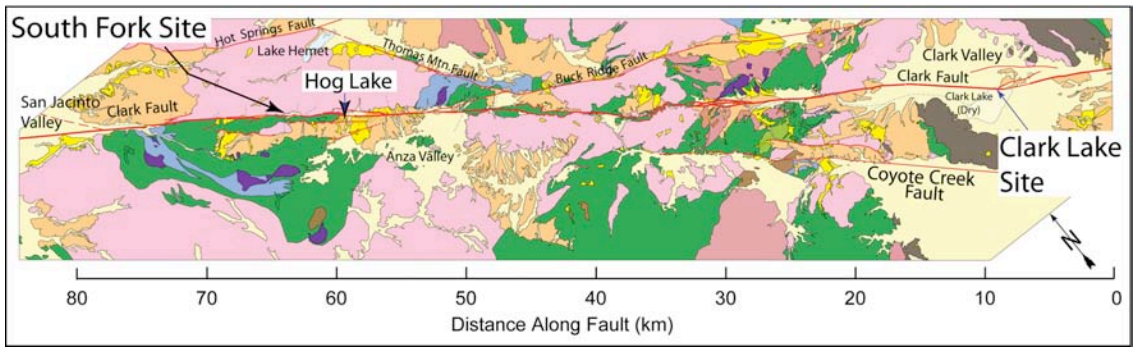

Figure 5. *Geological map of the central San Jacinto fault zone from Hemet southeast to Clark Valley (from Sharp, 1967). Note the locations of the South Fork, Hog Lake and Clark Lake paleoseismic sites.*

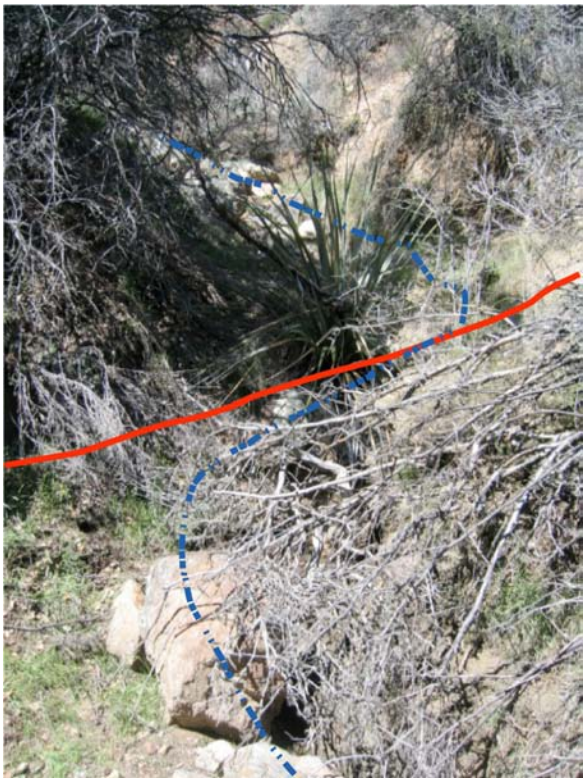

Figure 6. *Single event offset of a small channel in Burnt Valley, southeast of Anza. The red line is the fault, blue indicates the channel thalweg.*

In this section, we summarize the conclusions of these studies, but we include the entire manuscript of the combined work as an appendix: the manuscript has been submitted to the Bulletin of the Seismological Society of America (in review) for publication.

Small channels, alluvial bars, channel walls, rills, and other small-scale geomorphic features tend to be ephemeral features of the landscape. Large, infrequent storms obliterate these type and scale of features, essentially resetting the landscape, and their preservation is commonly related to how recently such a large storm has visited the region. Large earthquakes offset these small-scale features and can be recognized for several centuries after the earthquake event if they have not been obliterated by a large storm event (Figures 6 and 7). In southern California, several studies have used these types of features to measure discrete offset in the past one to several events (McGill and Sieh, 1991; Lindvall et al., 1989; Rockwell, 1990; Zilke et al., 2010), but rarely is there evidence for more than the past 4-5 events preserved along a fault, except the rare larger offset, which are commonly the focus for slip rate studies.

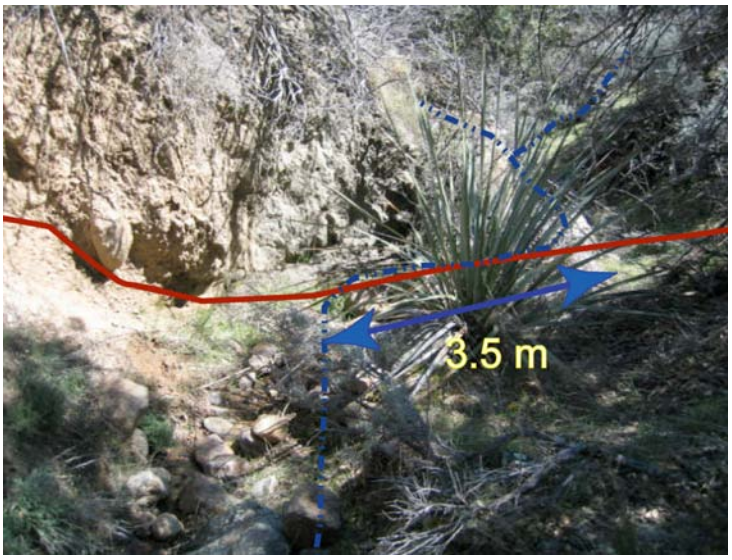

Figure 7. *Small, single event offset channel near Anza. Red line indicates fault, blue indicates the channel thalweg. Note that a scarp is still present at the channel margins along the fault.*

A common assumption for these studies is that displacements from a single earthquake will group along sections of the rupture, and that the group of smallest offsets is interpreted to represent slip in the most recent event. Mapping after the Landers earthquake (McGill and Rubin, 1999) demonstrated that along en echelon breaks, it is possible to get a bi-modal distribution of offsets, as they did for slip in 1992. From these and other observations, it appears best to use displacement values from only the simple, straight sections of a fault so as not to mix minor multiple-event displacements on secondary strands with the offsets along the primary fault.

For the Clark strand of the San Jacinto fault, we measured nearly 550 offsets on over 200 discrete features to determine slip in the past several earthquakes. Each offset was identified in aerial photography, LiDAR data or in the field, and each was measured by multiple means, where possible, but all were measured in the field. This required walking the entire length of the Clark fault from the San Filipe Hills northwest for about 85 km to where the fault enters the young alluvium at the mouth of Blackburn Canyon near Hemet.

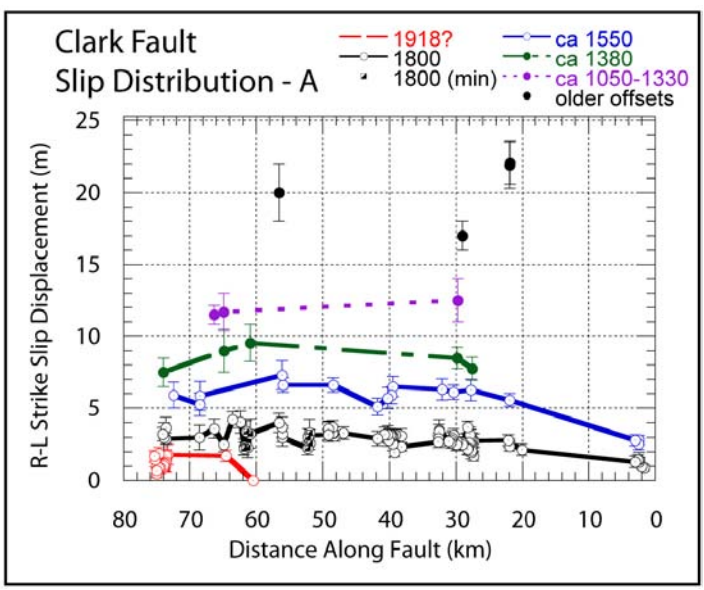

Figure 8. *Slip distribution of late Holocene surface ruptures from large earthquakes on the Clark strand of the central San Jacinto fault (Salisbury et al., 2011 in review).*

Each offset feature was rated based on its abruptness of offset, how well it could be located on the main trace of the fault from field exposures, and whether there was evidence of post-offset erosion that would affect the measurement result. For the final analysis, we used only the very good and excellent measurements, which were then plotted along the length of the Clark fault (Figure 8). In figure 8, note that the southeast end of the mapping area does not coincide with the southeast end of the Clark fault. We mapped offsets only from Lute Ridge

northwest to the mouth of Blackburn Canyon. Southeast of Lute Ridge, the fault begins to splay and become multiple stranded, and offsets on individual strands are less than a meter, which is too small to map or measure from the LiDAR data. Based on the presence of young scarps, we infer that these ruptures extended another 10-12 km to the southeast, terminating as bedding plane faults within the strongly folded Plio-Quaternary section of the San Filipe Hills. To the northwest, the fault is buried by active alluvium at the mouth of Blackburn Canyon, so no small geomorphic offsets were recognized farther to the northwest into the San Jacinto basin and step-over.

Several important conclusions are derived from these observations. First, the observations tend to cluster in areas of steep topography with increased slope aspect, and are absent or very difficult to recognize in areas of low topography (valleys) and areas of active alluviation. Consequently, there are gaps in data collection along the fault where preservation of small offsets is poor or absent.

Second, displacement near Anza and Hog Lake reaches a maximum of about 3.5 - 4 m, which we take to be the maximum displacement in the most recent event (Hog Lake is at km 58, Anza is at ~km 50). This event at Hog Lake is dated to ca 1790 and matches the sparse historical accounts of an earthquake recorded at San Juan Capistrano and San Diego on November 22, 1800. We therefore infer that we have located the surface rupture for this early historical earthquake. The larger offsets represented by the blue band are attributed to the penultimate event, which at Hog Lake is dated to ca AD 1550. This implies that this earlier Hog Lake event was similar in size to the most recent event in 1800, as cumulative displacements reach a maximum of about 7 m near Anza. Similarly, larger offsets are attributed to three or more events and may correspond to the Hog Lake events between AD 1000 and 1400.

Towards the northern part of the mapped section of fault, we recognize some smaller displacements in Blackburn Canyon itself. In some cases, these small displacements are adjacent to larger ones, and they are apparently younger based on the freshness of the geomorphology. We speculate that these offsets were produced by the M6.9 1918 earthquake, which to date has not been ascribed to a specific rupture. Early geologists searched for a rupture, but their track line skipped the entirety of Blackburn Canyon in favor of the easier route up Bautista Canyon. It is this observation that spurred our interest in opening a trench in the difficult to access South Fork Wilderness Area, as discussed in the next section.

In summary, the mapping of geomorphic offsets has led to a far better understanding of the paleoseismic record at Hog Lake. The past three Hog Lake earthquakes appear to all be large. From the extent of rupture, these each ruptured a distance of at least 85 km, and more likely well into the San Jacinto basin for a rupture length of up to 120 km. Considering the depth of microseismicity along the Clark-Casa Loma fault, we estimate that these earthquakes were in the Mw7.3 range. We also recognize that the northern Clark fault apparently fails in smaller earthquakes, such as the M6.9 1918 San Jacinto earthquake, which points to the possibility that some such past events may have ruptured into the Anza Seismic Gap to Hog Lake. This may explain the cluster of three events between about AD 1300 and 1400 from the Hog Lake record. If correct, then only one of these likely produced the large displacements observed from the geomorphology. In this model, the northern Clark fault is relatively weak and may fail more frequently than the section of fault in the seismicity gap. These ideas and models can all be tested with additional work.

The South Fork Wilderness Site

A consequence of the mapping of small geomorphic offsets to map slip distribution was the recognition that a short, 20 km section of the fault in Blackburn Canyon has very young-appearing offsets, with average displacement of about 1.25 m, as discussed in the previous section. The most likely interpretation is that these represent the surface rupture from the 1918 earthquake, the only plausible source for the past 150 years. Towards resolution of whether this is the 1918 rupture source, we applied for and received (after 6 months) permission to trench in the South Fork Wilderness Area, with the stipulation that all access would be by foot, and that all excavations would be by hand.

The site we chose to trench has alluvium ponded against a shutter ridge (fault scarp), so the area looked like it had the potential for a good stratigraphic section. To reach the site requires descending about 350 m in elevation by foot with all tools necessary for the excavations. The remoteness precluded use of trench shores, so the trench was only excavated to a depth of 2 m with sloped walls.

The trench exposed a succession of relatively coarse sandy units (units 20 through 50) overlying silty strata (units 60 through 100) at about 1.5 m depth (Figure 9). The sandy section is capped by a weakly-formed buried A soil horizon (unit 30) plus an additional 20-30 cm of additional sandy sediment, and an organic-rich A horizon (unit 10) caps the surface deposits. At the fault, a peat-like horizon has developed in a small depression along the surface rupture from the most recent event. The fault zone is at least a meter wide, but all latest Holocene activity is limited to a zone that is less than 0.7 m in width.

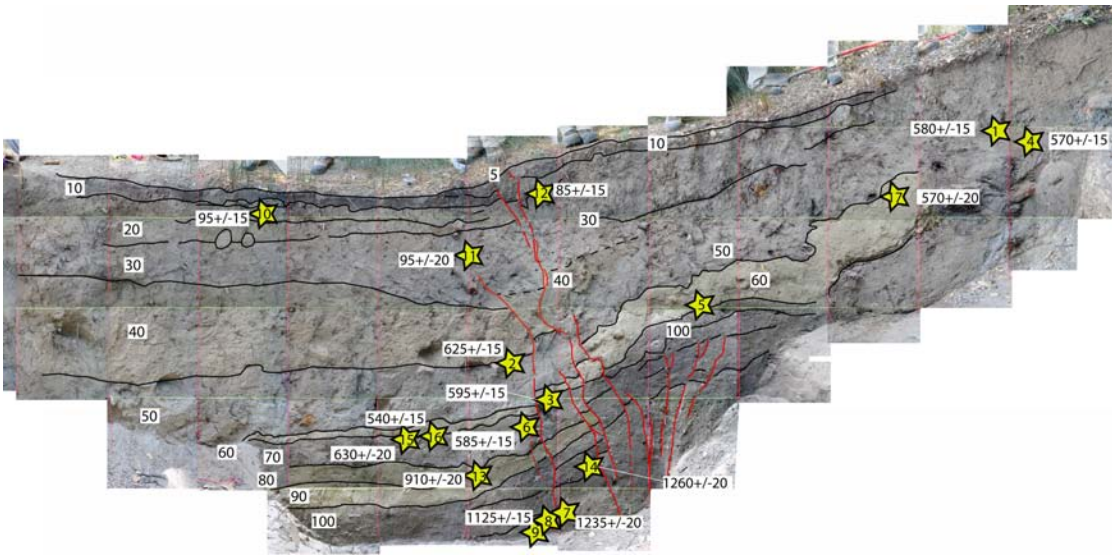

Figure 9. *Log and photomosaic of the SE wall of the South Fork Wilderness trench.*

The most recent event is recorded by rupture to the surface. The fault trace is difficult to recognize in the coarse sand of units 30 and 40, but is traceable where it

offsets the more bedded part of the section. There appears to be a fissure fill deposit in the fault zone, and the fault affects the surface by producing a graben that has accumulated a peat-like deposit at the base of a small scarp. All of these observations indicate that there has been no deposition at this site since the most recent event. Considering the weakness of the surface soil, these observations are consistent with a 1918 age for this event, but do not preclude the November 1800 earthquake either. Samples for pollen analysis were collected from the upper 2 cm of peaty sand, as well as at several intervals downward to a depth of a meter, to test for the presence of historically introduced pollen.

The penultimate event is indicated by rupture and upward splaying of fault strands into the sandy section of units 30 and 40, whereas units 10 and 20 display no disturbance and appear unfaulted by this splay. Unit 30 thickens into the main fault zone, which is interpreted to represent the position of the event horizon (surface at the time of the rupture) with the thickening due to scarp degradation. An earlier event is represented by several fault splays that offset unit 100, but are capped by the uppermost part of unit 100, as well as unit 60.

We dated fifteen samples of detrital charcoal recovered from the faulted section. Remarkably, all dates lie in stratigraphic order, or nearly so. Units 10 through 30 yielded dates that calibrate to younger than AD 1700, whereas units 50 through 70 yield dates that calibrate to the AD 1400 to 1600 year period. The oldest dates are on samples from unit 100 and indicate that the entire exposed section records about a thousand years of sedimentation.

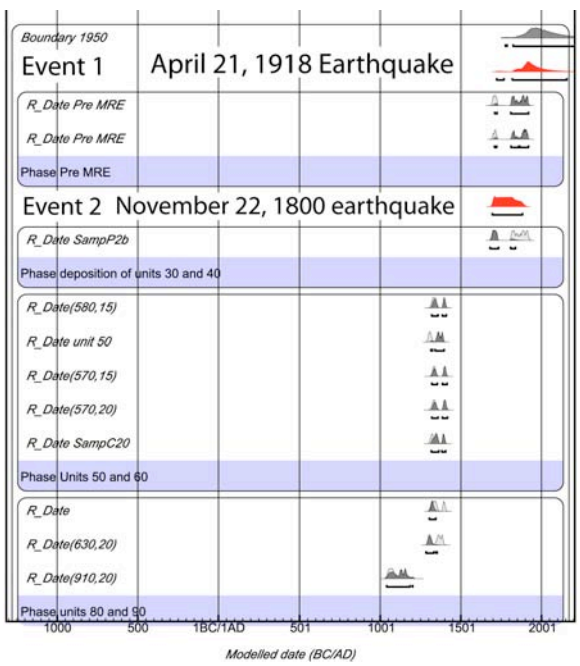

Figure 10. *OxCal plot of radiocarbon ages and calculated age of events 1 and 2.*

At face value, it appears that both of the two most recent events occurred after AD 1700. We placed the dates in OxCal (Bronk-Ramsey, 2010) to place age constraints on the ages of events 1 and 2 (Figure 10). The resulting analysis argues strongly that this section of fault has sustained rupture twice in the past 300 years, whereas the Hog Lake record only recognizes the occurrence of a single rupture in the same time period, with the penultimate event at about AD 1550. The age of the third event at the South Fork trench is consistent with the penultimate Hog Lake event. These observations strongly support the contention that the 1918 earthquake produced rupture along the northern Clark fault, as suggested by the geomorphology (Salisbury et al., 2011 in review).

The Clark Lake Paleoseismic Site

Clark Lake is a closed depression along the southern third of the Clark fault. Based on the rupture mapping from the geomorphic offsets, the past 2-3 earthquakes at Hog Lake should be represented by ruptures through Clark Lake, so developing an independent rupture history at Clark Lake will test the Hog Lake record at the same time we test the rupture distribution model derived from the geomorphology.

Multiple strands of the fault are mapped through the area of the lake (Figure 10), which made this site particularly interesting from the perspective of dating events. In addition, playas commonly have abundant detrital charcoal that washes from higher

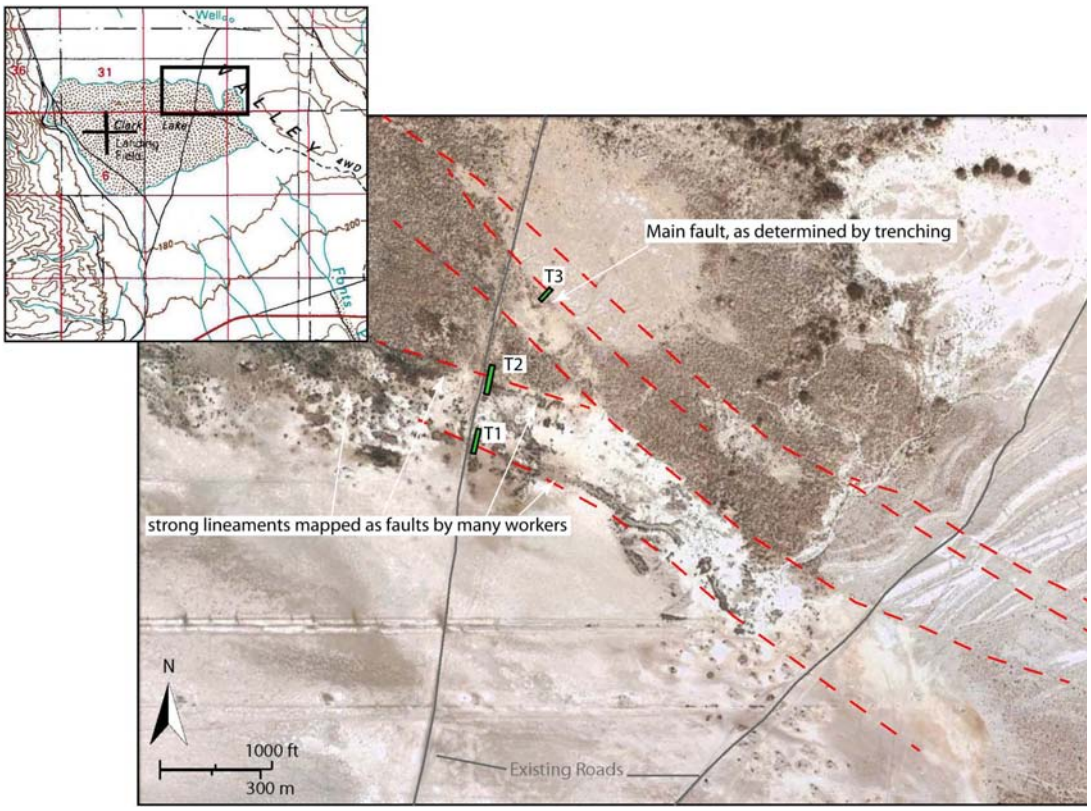

Figure 10. *Location of trenches excavated in Clark Lake playa. Trenches 1 and 2 were dug across two prominent lineaments in the lowest part of Clark Lake. Trench 3 was excavated across a scarp. Faulting exposed in trenches 1 and 2 was minor, whereas trench 3 exposed the main fault.*

elevations after fires or is derived from local archeological sites. Indeed, a major archeological site is present within a few hundred meters to the northeast of the fault, so fire remains should be abundant.

Clark Lake was designated as a State Wilderness Area in 2007, which requires that all work be done by hand. Normally, access would also have been by foot but there were existing roads that we were allowed to use for access. We expected the lowest area to have the highest deposition rate, and therefore the best record of faulting, so we initially began excavating trench T1 in a depression with active sedimentation. Indeed,

during a storm event in January, the trench filled with water as this area of the depression was inundated. However, we encountered only minor faults and cracking to a depth of 1.5 m, and preliminary radiocarbon analysis indicated that the strata at the base of the trench were on the order of 2,000 years. Considering the expected recurrence interval on the order of hundreds of years, and the lack of clearly defined events, we opened trench T2 across the adjacent lineament, that together with trench T1, extended the excavations to a combined length of more than 100 m. Again, we exposed only minor faulting, which strongly indicates that neither of these lineaments represents the primary fault trace. Finally, we opened a short trench, T3, across the third lineament represented by a low, 20 cm high scarp and exposed a major fault, which we now interpret as the main strand.

Trench T3 exposed well-stratified lacustrine and fluvial sediments juxtaposed against massive, older playa sediments (Figures 11 and 12). Preliminary radiocarbon analysis of detrital charcoal revealed that the massive sediments on the northeast side of the fault are on the order of 3 ka, whereas the section on the southwest side are on the order of modern to 1500 years in age. Of significant note is that the majority of radiocarbon dates are apparently too old relative to other sample ages, which indicates a

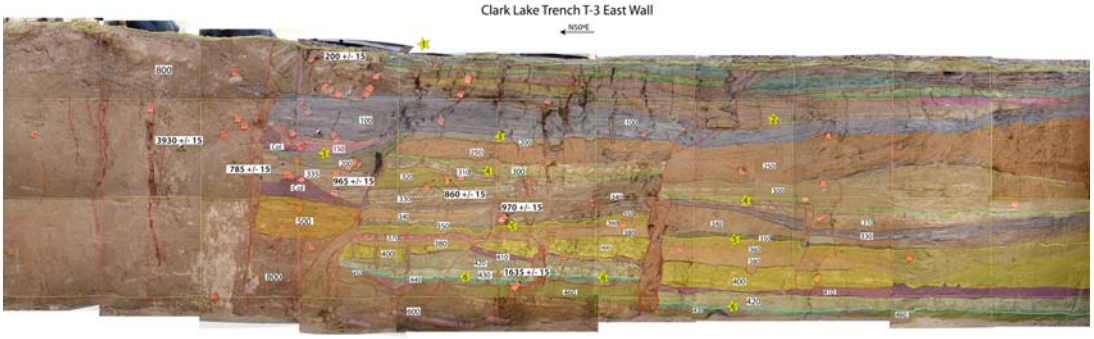

Figure 11. *Log of the SE wall of trench T3 in Clark Lake playa.*

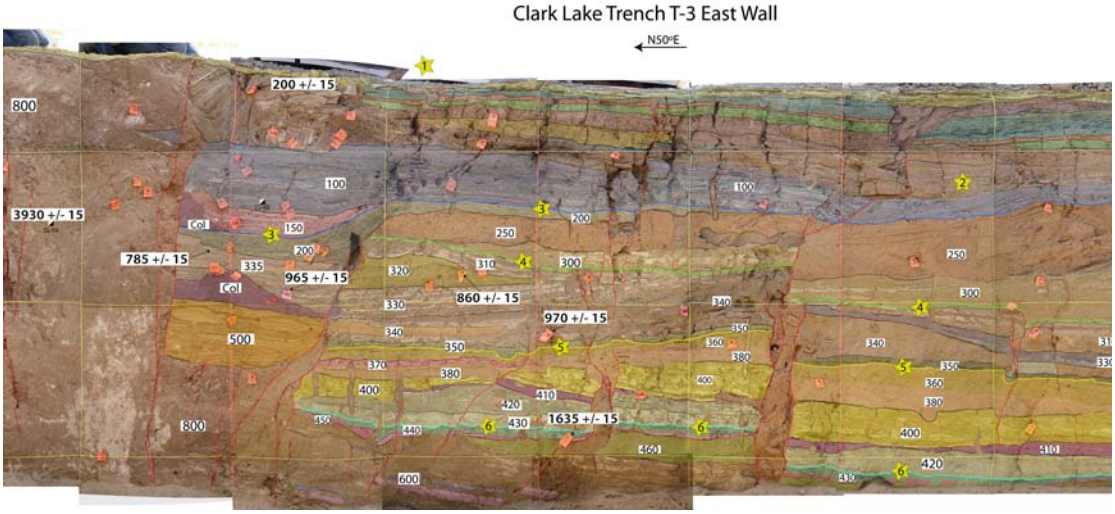

Figure 12. *Detail of fault zone of Clark Lake T-3. Stars with numbers indicate locations where evidence is present for the six surface rupturing events. Ages for detected radiocarbon dates that do not violate stratigraphic ordering are shown.*

substantial component of inheritance or burning of old wood. Most of the samples are probably derived from a nearby archeological site, so the occurrence of old charcoal is expected. Nevertheless, it may require as many as 100 dates to eventually nail down the chronology sufficiently so as to match that at Hog Lake.

Evidence for six surface ruptures (stars in figures 11 and 12) are apparent in the upper 1.5 m of stratigraphy, based on upward termination of major fault splays, fissures and fissure fills, angular unconformities where tilted stratigraphy is overlain by flat-lying stratigraphy, and the abrupt decrease in vertical separation at a specific horizon. In fact, each interpreted event shows most of these factors, which strongly argues that these observations are evidence of bonafide earthquakes that ruptured to the paleo-ground surface.

The current chronology is not well enough constrained for direct comparison of all events to those at Hog Lake. Nevertheless, all six events have occurred within the past 1500 years, and five appeared to have occurred in the past 1000 years. As many as seven events are recognized for the past 1 ka time period at Hog Lake, with only one additional event to 1500 years. The most recent event at Clark Lake dates to younger than AD 1680, consistent with the geomorphology that argues that the most recent event at both Hog Lake and Clark Lake are the same event. We therefore correlate events E1 at both sites to the November 22, 1800 earthquake that is well-dated at Hog Lake.

A potentially important issue relates to the cluster of three events at Hog Lake between about AD 1290 and 1400 (1292, 1332, 1383). If each of these events is large and similar in slip distribution to the November, 1800 earthquake, we would expect to see evidence for each of these events at Clark Lake. In contrast, we see evidence for only one event in the timeframe of the Hog Lake cluster, which suggests that two of them were either smaller, or ruptured to the north similar to the 1918 rupture (Benzion et al., 2011 in review; Salisbury et al., 2011 in review). Continued dating at Clark Lake should more accurately resolve which of the Hog Lake events produced slip at Clark Lake.

Conclusions

The paleoseismic record at Hog Lake has been further clarified by new trenches in the South Fork Wilderness Area to the northwest of Hog Lake, and at Clark Lake Wilderness Area to the southeast. Mapping of slip distribution for the past several ruptures has developed evidence that the 1918 earthquake produced rupture in Blackburn Canyon between Hog Lake and Hemet. Trenching has confirmed the occurrence of two ruptures along the fault in Blackburn Canyon after AD 1700, whereas only one event is recognized at Hog Lake for this period. The Clark Lake paleoseismic record records evidence of most of the Hog Lake events, but yields evidence for only one event in the AD 1300 timeframe, during which a cluster of three events are noted at Hog Lake. These observations, taken together, are most simply explained if two of the events in the cluster are similar to the 1918 rupture, with some displacement into the Anza Seismic Gap at Hog Lake. Additional dating at Clark Lake will further shed light on understanding the late Holocene pattern of earthquakes along the Clark strand of the San Jacinto fault.

References Cited

Ben-Zion, Y., T. K. Rockwell, Z. Shi, and S. Xu, 2011 in review, Reversed-polarity secondary deformation structures near fault step-overs, submitted to Geophysical J. Internat., March, 2011.

Bronk-Ramsey, 2010, Radiocarbon program OxCal version 4, available at https://c14.arch.ox.ac.uk/login

Klinger, Ralph E. and Rockwell, Thomas K., 1989, Recurrent late Holocene faulting at Hog Lake in the Anza seismic gap, San Jacinto fault zone, southern California: Geological Society of America, Abstracts With Programs, v. 21, no. 5, p. 102.

Lindvall, S.C., Rockwell, T.K., and Hudnut, K.W., 1989, Evidence for prehistoric earthquakes on the Superstition Hills fault from offset geomorphic features: Seismological Society of America Bulletin, v. 79, no. 2, p. 342-361.

Middleton, T.J., 2006, Tectonic geomorphology of the southern Clark fault from Anza southeast to the San Felipe hills: Implication of slip distribution for recent past earthquakes, 95 p.

McGill, S.F. and Sieh, K., 1991, Surficial offsets on the central and eastern Garlock fault associated with prehistorical earthquakes. J. Geophys. Res, v. 96, B13, p. 21,597-21,621.

McGill, S.F. and Rubin, C.M., 1999, Surficial slip distribution on the central Emerson fault during the June 28, 1992 Landers earthquake, California. J. Geophys. Res, v. 104, B3, p. 4811-4833.

Onderdonk, N., S. McGill, G. Marliyani, and T. Rockwell, 2010, Preliminary results from Mystic Lake: A new paleoseismic site along the northern San Jacinto fault zone. Southern California Earthquake Center (SCEC) Annual Meeting Proceedings and Abstracts, v. 20, p. 258.

Pandey, A. and Rockwell, T.K., 2011 in progress, Slip distribution for the most recent surface ruptures along the northern Coyote Creek fault, southern California. To be presented at the SCEC annual meeting, Palm Springs, 2011.

Ragona, D., Rockwell, T.K., and Orgil, A., 2001, Fault segmentation and earthquake behavior: A high-resolution paleoseismic study in the southern San Jacinto fault zone. Eos Trans. AGU, 83(47), Fall Meet. Suppl., Abstract S52D-0668.

Rockwell, T., 1990, Holocene activity of the Elsinore fault in the Coyote Mountains, southern California: in Western Salton Trough Soils and Tectonics, Friends of the Pleistocene Guidebook, p. 30-42.

Rockwell, T.K., J.A. Dewhurst, C.W. Walls, W.J. Pollard, A. Orgil, G. Faneros, and T.E. Dawson, 2000, High-resolution paleoseismology in southern California: Investigation of segment controls on the rupture history of the southern San Jacinto fault: in Active Fault Research for the New Millenium, Proceedings of the Hokudan International Symposium and School on Active Faulting, (K. Okumura, K Takada, and H. Goto, eds.), Letter Press Ltd., Hiroshima, Japan, p. 413-419.

Rockwell, T.K., J. Young, G. Seitz, A. Meltzner, D. Verdugo, F. Khatib, D. Ragona, O.

Altangerel, and J. West, 2003. 3,000 years of ground-rupturing earthquakes in the Anza Seismic Gap, San Jacinto fault, southern California: time to shake it up?, Seismological Research Letters 74, pp. 236-237.

Rockwell, T.K., Seitz, G., Ragona, D.E., Dawson, T.E., Faneros, G., Verdugo, D., and Altangerel, O., 2005, Investigation of segment controls on the rupture history of the southern San Jacinto fault. Seismological Research Letters, v. 76, no. 2, p. 254.

Rockwell, T., Seitz, G., Dawson, T., and Young, J., 2006, The long record of San Jacinto fault paleoearthquakes at Hog Lake: Implications for regional strain release in the southern San Andreas fault system. Seismological Research Letters, v. 77, no. 2, p. 270.

Salisbury, J.B., Rockwell, T.K., Middleton, T.J., and Hudnut, K., 2011 in review, LiDAR and Field Observations of Slip Distribution for the Most Recent Surface Ruptures Along the Central San Jacinto Fault. Submitted to Bulletin of the Seismological Society of America, March 1, 2011.

Verdugo, D.M., Ragona, D.E., and Rockwell, T.K., 2005, Further resolution of paleoseismicityy at the Carrizo Wash site, Superstition Mountain strand of the San Jacinto fault, Imperial Valley, southern California. Seismological Research Letters, v. 76, no. 2, p. 254.

Zilke, O., Arrowsmith, R., Grant-Ludwig, L. and Akciz, S.O., 2010, Slip in the 1857 and Earlier Large Earthquakes Along the Carrizo Plain, San Andreas Fault. Science 327, 1119 DOI: 10.1126/science.1182781

Editorial Manager(tm) for Bulletin of the Seismological Society of America
Manuscript Draft

Manuscript Number:

Title: LiDAR and Field Observations of Slip Distribution for the Most Recent Surface Ruptures Along the Central San Jacinto Fault

Article Type: Article

Section/Category: Regular Issue

Corresponding Author: James Barrett Salisbury, M.S.

Corresponding Author's Institution: San Diego State University

First Author: James Barrett Salisbury, M.S.

Order of Authors: James Barrett Salisbury, M.S.;Thomas K Rockwell, Ph.D.;Timothy J Middleton, M.S.;Kenneth W Hudnut, Ph.D.

Abstract: We measured offsets on tectonically displaced geomorphic features along 80 km of the Clark strand of the San Jacinto fault (SJF) to determine slip per event for the past several surface ruptures. We identify 203 offset features from which we make over 560 measurements using B4 LiDAR imagery, field observations, and aerial photography. Displacement estimates suggest that the most recent surface-rupturing event (MRE) produced an average of 2.5-2.9 m of right-lateral slip with maximum slip of nearly 4 m at Anza - a Mw 7.2 to Mw 7.5 earthquake. Double-event offsets for the same 80 km section average ~5.5 m of slip, with maximum values of 3 m at Anza for the penultimate event. Cumulative displacements of 9-10 m through Anza suggest the third event was also similar in size. Paleoseismic work at Hog Lake dates the most recent surface rupture event at ca. 1790. A poorly located, large earthquake occurred on November 22, 1800, causing extensive damage (MMI VII) at San Diego and San Juan Capistrano missions. We relocate this event to the Clark fault based on the MRE at Hog Lake. We also recognize the occurrence of a younger rupture along ~15- 20 km of the fault in Blackburn Canyon with ~1.25 m of average displacement. We attribute these offsets to the Mw 6.9 April 21, 1918 event. These data argue that much or all of the Clark fault, and possibly also the Casa Loma fault fail together in large earthquakes, but that shorter sections may fail in smaller events.

Suggested Reviewers: Sinan Akciz
sakciz@uci.edu
Familiar with this type of work

Sally McGill
smcgill@csusb.edu
Familiar with this type of work

Ramon Arrowsmith
ramon.arrowsmith@asu.edu
Familiar with this type of work

Opposed Reviewers:

Letter to Editor
Click here to download Letter to Editor: CoverLetterBSSA(JBS).pdf

SAN DIEGO STATE UNIVERSITY
San Diego State University
Department of Geological Sciences
College of Sciences
San Diego State University
San Diego, CA 92182-1020

TEL: (619) 594-5586
FAX: (619) 594-4372

Diane I. Doser
Editor-in-chief, BSSA

March 1, 2011

Dear Dr. Doser,

We are pleased to submit our manuscript entitled "LiDAR and Field Observations of Slip Distribution for the Most Recent Surface Ruptures Along the Central San Jacinto Fault" to the Bulletin for consideration for publication. This work culminates nearly five years of field mapping and remote analysis of tectonically displaced geomorphic features along the Clark strand of the San Jacinto fault zone in southern California. We present new slip-per-event data for the past several surface ruptures, relocating the significant (M*w* 7.2-7.5) yet poorly located earthquake of November 22, 1800 to the Clark fault. Additionally, we recognize the presence of a previously unmapped surface rupture of the earthquake of April 21, 1918 (M*w* 6.9) through Blackburn Canyon. Our geomorphic observations argue for fairly characteristic slip along the Clark fault for at least the past three events. We believe that these new observations will be of broad interest to the hazards community in southern California and elsewhere.

Sincerely,

James Barrett Salisbury, M.S.
Corresponding Author

*Manuscript
Click here to download Manuscript: Salisbury_et_al_2011_manuscript.pdf

LiDAR and Field Observations of Slip Distribution for the Most Recent Surface Ruptures Along the Central San Jacinto Fault

J. B. Salisbury[1]

T. K. Rockwell[1]

T. J. Middleton[1]

K. W. Hudnut[2]

[1]Department of Geological Sciences, MC-1020

5500 Campanile Drive

San Diego State University

San Diego, CA 92182

USA

[2]U.S. Geological Survey

525 South Wilson Avenue

Pasadena, CA 91106

USA

Online Material: Annotated topographic contour maps and hillshades derived from raw and filtered B4 LiDAR data, corresponding field photographs, and data tables comparing LiDAR-based and field-based slip measurements for individual geomorphic features along the Clark fault.

Abstract

We measured offsets on tectonically displaced geomorphic features along 80 km of the Clark strand of the San Jacinto fault (SJF) to determine slip per event for the past several surface ruptures. We identify 203 offset features from which we make over 560 measurements using B4 LiDAR imagery, field observations, and aerial photography. Displacement estimates suggest that the most recent surface-rupturing event (MRE) produced an average of 2.5-2.9 m of right-lateral slip with maximum slip of nearly 4 m at Anza – a M*w* 7.2 to M*w* 7.5 earthquake. Double-event offsets for the same 80 km section average ~5.5 m of slip, with maximum values of 3 m at Anza for the penultimate event. Cumulative displacements of 9-10 m through Anza suggest the third event was also similar in size. Paleoseismic work at Hog Lake dates the most recent surface rupture event at ca. 1790. A poorly located, large earthquake occurred on November 22, 1800, causing extensive damage (MMI VII) at San Diego and San Juan Capistrano missions. We relocate this event to the Clark fault based on the MRE at Hog Lake. We also recognize the occurrence of a younger rupture along ~15-20 km of the fault in Blackburn Canyon with ~1.25 m of average displacement. We attribute these offsets to the *Mw* 6.9 April 21, 1918 event. These data argue that much or all of the Clark fault, and possibly also the Casa Loma fault fail together in large earthquakes, but that shorter sections may fail in smaller events.

Introduction

The distribution of displacement resulting from surface rupture during a moderate to large earthquake closely correlates to the magnitude of the earthquake (Wells and Coppersmith, 1994). Many ruptures offset rills, small channels, alluvial bars and other features that can be preserved in the landscape for centuries or more. Mapping of these small offset features has allowed for the documentation of slip distribution of many early or prehistoric earthquakes, and has allowed for an estimate of the size of these events (e.g. Sieh, 1978; Rockwell and Pinault, 1986; Lindvall et al., 1989; Rockwell, 1990; McGill and Sieh, 1991; McGill and Rubin, 1999; Kondo et al., 2005; Zielke et al., 2010).

The San Jacinto fault (SJF) zone is a major component of the overall southern San Andreas Fault (SAF) system, and together these regional structures accommodate as much as 80% of the Pacific-North America relative plate motion in southern California - 25-40% of which may occur on strands of the SJF alone (DeMets and Dixon, 1999; Bennett et al., 2004; Fialko, 2006). Although the SJF zone comprises many discrete faults, the Clark-Casa Loma strand is the longest and most continuous segment at nearly 120 km in total length, stretching from the San Felipe Hills in the western Salton Trough northwest to the San Jacinto Valley (Fig. 1) (Sharp, 1967; Rockwell et al., 1990; Matti et al., 1992; Morton and Matti, 1993; Blisniuk et al., in prep).

The slip rate of the SJF zone has been estimated to range between 8 and 23 mm/yr since the mid-Quaternary (Sharp, 1967; Sharp, 1981; Rockwell et al., 1990; Morton and Matti, 1993; Janecke et al., 2004; Dorsey, 2002; Rockwell et al., 2006; Blisniuk et al., in prep), with the Holocene rate near Anza being estimated at about 16.3 ± 4.7 mm/yr for the past 4.3 ka (Merifield et al., 1991; Blisniuk et al., in prep). The large discrepancies between geologic slip-rates are ascribed to the along-strike location of the offset feature or paleoseismic site, the type of geomorphic feature being dated, and the time scale over which the dated displacement occurred. Some of the slip rates have been determined on fault strands that carry only a percentage of the total SJF slip (Blisniuk et al., in prep). The Holocene rate at Anza is significant because nearly all of the total fault slip is on the Clark fault; so 16 mm/yr appears to be the current rate of strain release along this section of the SJF. Assuming elastic rebound satisfactorily describes the energy release in surface-rupturing earthquakes, and that geomorphic features form more frequently than these earthquakes, using this Holocene slip rate in combination with information on slip per event can provide insight to the average time between large earthquakes (the recurrence interval). This interval can provide a crosscheck to direct dating of past surface ruptures using paleoseismic techniques (Rockwell et al., 2006).

Methods

We divided the south central 80 km Clark fault into nine major sections where strike-slip evidence is most prevalent and best preserved (Fig. 2). These sections generally correspond to remote and isolated areas of the fault zone where the geomorphology is pristine and undisturbed. The divisions between sections are composed of structural complexities, areas of young alluvium, gorges, and near Anza, the Ramona Indian Reservation. For each of these sections, the thalwegs of small channels, channel margins, bar crests, and ridge noses were measured to estimate displacement for each feature, and these were compiled to generate the slip distribution for the last three surface ruptures.

For the entire field area, we utilize B4 Light Detection and Ranging (LiDAR) data to create high-resolution bare earth digital elevation models (DEM's) with which to analyze the tectonic geomorphology of the Clark fault at multiple scales (100's of meters to sub-meter scale). The B4 LiDAR dataset was acquired in May 2005 as a pre-earthquake survey of the SAF and SJF zones in southern California. The dataset is intended for comparison of pre- and post-earthquake LiDAR after a large earthquake so that the field of ground-surface deformation can be quantified remotely (see Data and Resources section).

Along strike, the SJF varies greatly in elevation, from 200-300 m in Clark Valley to over 1200 m NW of Anza Valley. In addition to variations in terrain and elevation, average annual rainfall and vegetation density also vary along strike

accordingly. Along the southern half of the study area, the arid climate of the Salton Trough dominates, so sparse vegetation required only minimal filtering of the B4 LiDAR data set. In contrast, dense vegetative cover (Manzanita, scrub oak, live oak, sagebrush, yuccas, Joshua pines, and annual grasses) near and to the northwest of Anza Valley presented a formidable challenge to the recognition and mapping of offset features, both in the field and by remote data analysis. Finally, most of the field area between Rockhouse Canyon and Burnt Valley, as well as northwest of Anza to Hemet, is remote and accessible principally by foot, which made some of the fieldwork challenging.

In areas of higher elevation where vegetation is dense, we used an iterative, multi-scale curvature classification algorithm in Environmental Systems Research Institute's (ESRI's) ArcInfo/Workstation to manually remove vegetation from raw point clouds, similar to the technique of Evans and Hudak (2007). Contour maps with 0.25 m intervals were created in ESRI's ArcMap v9.3 for each of the nine fault sections, and displaced geomorphic features were analyzed using Applied Imagery's Quick Terrain Modeler (QTM) v7.1.2. and the MATLAB graphical user interface (GUI) LaDiCaOZ.

Methods used to measure displaced features in QTM were analogous to geomorphic methods used in the field: by matching similar features such as channel margins and thalwegs that intersect and are nearly perpendicular to the fault and measuring the tectonic separation of these features along the strike of the fault. For channel features that lack distinctive piercing lines (such as

channel margins or thalwegs) directly into the fault, piercing lines are projected into the fault zone and slip is measured along strike of the fault. A minimum of three slip measurements were made for each offset feature in QTM: an ideal slip value, a minimum accepted value, and a maximum accepted value. In some cases, a single feature required nine individual measurements – a separate average for the ideal, minimum and maximum values. The largest difference between the ideal value and accepted minimum or maximum value was used to assign the uncertainty to the ideal displacement measurement (e.g. Zielke et al. 2010). Where offset features are appreciably larger than the resolution of the filtered LiDAR data, we also use the MATLAB graphical user interface (GUI) LaDiCaOZ to assess displacement magnitudes (Zielke et al., 2010).

The locations of all offset features identified in filtered point clouds were visited and measured in the field as a means of filtered LiDAR validation. A Panasonic Toughbook CF-19 Tablet-GPS combination computer was used for the fieldwork, and offset features were located and placemarked on-site in Google Earth using the constructed 0.25 m GeoTiff contour maps. Slip measurements and associated uncertainties were estimated in the field using a metric measuring tape. To aid with the measurements, offset channel features were defined with colored string and photographed with a scale.

Sieh (1978) used a quality rating system of excellent, good, fair, and poor to rate identified offset features. We translated this scale to a numeric rating system from one to ten (0-5 = Poor, 5.25-6.75 = Fair, 7-8.75= Good, and 9-10 =

Excellent). The quality of field measurements and measurement uncertainties are based upon: feature distinctiveness, the prominence of the fault trace, the average size of alluvial material, the degree to which features were projected into the fault trace, the degree of feature degradation, and the density of surrounding vegetation (which limited visibility considerably in some areas).

The quality of LiDAR-based measurements is also assessed in a similar fashion. However, each respective characteristic is based upon the quality of the 0.25 m contours generated from the filtered B4 LiDAR data. Therefore, every feature identified in the LiDAR DEM's was visited and measured in the field.

In an area where displacement estimates cluster around distinctly separate magnitudes (particularly where the larger values are multiples of the smallest value) we infer that the larger magnitude displacements are a result of multiple earthquakes. The minimum cluster value is attributed to offset from the most recent event (MRE) in that area, and subsequently larger clusters are attributed to the displacement incurred in multiple paleoearthquake events. Where clusters of large displacement are found, we infer that multiple earthquakes occurred to produce the larger offsets.

Observations

Although there are several fault strands mapped throughout the entire study area (Sharp, 1967; 1972), in most cases, we were able to locate the most recently active strands on which the majority, if not all of the recent slip has occurred. We present over 560 individual measurements made from 203 fault-offset geomorphic features along the 80 km segment of the Clark fault (Fig. 3, Table 1). Examples of B4 LiDAR products and field photographs of offset features can be seen in Appendix A in the electronic supplement to this article. For this section, offset measurements are discussed by study area along strike, starting in the southeast at Lute Ridge which we term km-point zero. Locations along the fault are cited as "X" km northwest from this arbitrary point, southeast of which we could not effectively measure displacements using LiDAR data. It should be noted that scarps with small displacements along the fault continue for an additional 10-12 km to the southeast, but that displacements of less than a meter can be ambiguous and difficult to quantify with B4 LiDAR data or even field measurements. In addition, the fault splays to the southeast, so offset estimates would likely be minimum values.

Lute Ridge

Lute Ridge is the southernmost fault section evaluated for tectonic offsets, located a few kilometers from the mapped termination of the Clark fault where

multiple splays enter the San Felipe Hills (Fig. 2) (Sharp, 1967; Sanders et al., 1986; Janecke et al., 2004). The surface trace of the fault is discontinuous, but the main strand is mapped at the base of the steep, NE face of Lute Ridge with displacement estimated on well-developed, deeply incised rills through unconsolidated alluvium. This section has an average elevation of 300 m, and from km-point 1.65 to 3.03 we investigated 17 locations and found 22 measurable offset features. The 35 total field and LiDAR-based measurements from this area are listed in Table 1 and can be seen in Figure 4.

The average slip measured for the MRE is ~1.3 m in this area, with individual field measurements ranging from less than a meter toward the southeast to ~1.5 m in the northwest of Lute Ridge. On 11 of the 35 features, slip is measured to be almost double the MRE at ~2.7 m (individual measurements range from 2.5 to 2.9 m), and is attributed to slip accrued in the past two events. Although only one offset was measured in the field (3.9 ± 0.7 m with a quality rating of 6/10), it is interpreted as the cumulative slip from the past three events (Fig. 3).

Rockhouse Ridge - Rockhouse Canyon

The Clark fault through Rockhouse Canyon and along Rockhouse Ridge is a continuous, 5-km-long, well-defined mole track through young alluvium that generally juxtaposes Cretaceous tonalite against Quaternary Bautista Formation (Fig. 2). Rill formation is rare, but within Rockhouse Canyon are two prominent

drainages with channels and bars preserving single and double-event offsets. This section has an average elevation of 300-650 m, and from km-point 18.58 to 22.16 we investigated 9 locations and found 11 measurable offset features. The 19 total field and LiDAR-based measurements from this area are listed in Table 1 and can be seen in Figure 5.

The average slip measured for the MRE is ~2.4 m in this area, with individual field measurements ranging from ~1.9 m in the southeast to ~2.7 m in the northwest. An average slip value of ~5.75 m for two features (a channel thalweg displaced 6 ± 0.4 m at km-point 19.1 and a bar crest displaced 5.5 ± 0.5 m at km-point 21.97) measured in the field is slightly more than double the MRE and is inferred to be slip from the past two events (Fig. 3). At two locations, we used only the LiDAR data to measure bar crests with large cumulative displacements of 22.1 ± 1.5 m and 21.9 ± 1.6 m at km-points 21.91 and 21.97, respectively.

Jackass Ridge

Along Jackass Ridge, the fault trace is a continuous 2-3 m wide bench across steep topography juxtaposing different elements of the Quaternary Bautista Formation (Fig. 2). A high density of drainages and fresh rills exist along this 1-km section, with the majority of recent slip between the front and back edges of the bench. This section has an average elevation of 700-900 m, and from km-point 27.31 to 29.05 we investigated 26 locations and found 67

measurable offset features. The 121 total field and LiDAR-based measurements from this area are listed in Table 1 and can be seen in Figure 6.

Variance in slip measurements throughout the steep area is attributed to large boulders clogging channel thalwegs. Average slip measurements for this section are ~2.5 m for the MRE, with individual field measurements ranging from 1.6 to 3.9 m. Slip in double-event offsets averages ~5.6 m with individual field measurements ranging from 5.3 to 7 m (Fig. 3).

Dry Wash

Immediately northwest of Jackass Ridge, the Dry Wash segment is a slightly transpressive, continuous and linear section with exposed fault geomorphology localized along the southwest side of the valley (Fig. 2). This section has an average elevation of 900-1100 m, and from km-point 29.73 to 32.67 we investigated 18 locations and found 44 measurable offset features. The 64 total field and LiDAR-based measurements from this area are listed in Table 1 and can be seen in Figure 7.

Error estimates are larger here because of the large boulders (≥3 m) clogging channel thalwegs, and while the majority of features were measured in both the field and from LiDAR DEM's, five features were measured only in the LiDAR DEM's. Displacement data from this section form tight clusters around three distinct values: ~2.8 m for the MRE (individual field measurements ranging from 2.5 to 3.5 m), ~5.5 m for the past two events (individual field measurements

ranging from 4.6 to 6.5 m), and although only constrained by two field measurements, ~8.9 m for the past three events (Fig. 3). Additionally, we measured a bar crest in the field at km-point 29.05 with large cumulative displacement of 17 ± 1 m (confidence 8/10), and a channel thalweg at km-point 29.73 with large cumulative displacement measured at 12.5 ± 1.5 m (confidence 4.5/10) in the field and at 16 ± 2 m (confidence 4/10) in the LiDAR data.

Horse Canyon – White Wash

This ~4 km sublinear fault segment is between restraining bends to the southeast and northwest, although the northern bend appears to have been bypassed and is now fairly linear. The active trace is preserved as a few highly dissected benches and offset stream channels (Fig. 2). This section has an average elevation of 900-1050 m and generally sporadic vegetation. However, in areas where springs concentrate groundwater, cacti and yucca are very dense. From km-point 37.77 to 41.81 we investigated 18 locations and found 49 measurable offset features. The 64 total field and LiDAR-based measurements from this area are listed in Table 1 and can be seen in Figure 8.

The majority of our field measurements cluster at ~3 m, slightly larger than the MRE of the previous section, with individual field measurements as low as 1.1 m, but generally falling between 2.3 and 3.5 m. LiDAR DEM's were useful for resolving the far-field deflection at five separate locations. These measurements average ~5.7 m and are attributed to slip from the past two events. These

measurements were made with low confidence, and therefore may not reflect the true amount of slip (Fig. 3).

Anza Valley – Burnt Valley

The Anza – Burnt Valley section is the longest section, stretching from the SE end of Sagebrush Flat NW to the Ramona Indian Reservation (Fig. 2). Throughout this section, the Clark fault is generally linear with several local complexities. In some areas of Burnt Valley and at the SE end of Anza Valley, the fault is buried by Holocene alluvium. Before entering a small pressure ridge in Anza Valley, the active fault splays into at least two sub-strands in young alluvium. Additionally, the major Buck Ridge fault splays to the ESE before slip is re-consolidated to a single strand at the northwest end of this part of the study area. This section has an average elevation of 1200-1400 m, and from km-point 46.92 to 56.6, we investigated 22 locations and found 46 measurable offset features. The 71 total field and LiDAR-based measurements from this area are listed in Table 1 and can be seen in Figure 9.

Multiple-stranded segments excluded, slip in the MRE is highest along this section of the fault, with an average of ~3.3 m of offset, with field measurements ranging from 2.2 to 3.9 m. To the NW, where slip is consolidated onto a single strand, high-confidence double-event offsets average ~6.8 m of slip (Fig. 3). Additionally, we measure a ridge nose at km-point 56.6 with a large cumulative displacement of 20 ± 2 m (confidence 7/10) in the LiDAR data.

Horse Creek Ridge Drainage – Rouse Hill

Multiple linear fault strands are present In the SE portion of this section near Hog Lake and the Ramona Indian Reservation (Fig. 2) (Sharp, 1967). At the NW end of the section, slip is once again re-consolidated onto a single active strand. Where the fault is not eroded by active drainages, tectonic geomorphology is expressed as prominent side-hill benches, shutter ridges, and scarps through Holocene alluvium and crushed basement rocks. This wilderness section has an average elevation of 1250-1400 m and contains extremely dense vegetation. From km-point 60.91 to 68.54 we investigated 21 locations and found 30 measurable offset features. The 52 total field and LiDAR-based measurements from this area are listed in Table 1 and can be seen in Figure 10.

Displacement magnitudes of field measurements range from 1.5 m to as much as 4 m in this section, with many estimates of slip regarded as minimums where multiple strands are present (Fig. 3). For sections where two or more strands are present, and where we measure the same geomorphic feature across both strands, we subjectively sum the displacements in order to estimate displacement magnitudes in past events.

Blackburn Canyon

Blackburn Canyon represents the final 3 km along which we were able to map the tectonic geomorphology of the Clark fault (Fig. 2). The fault is mapped as a single, linear fault trace through an uplifted, crushed zone of varying

lithologies, and is expressed as prominent shutter ridges and side-hill benches on the northeast side of Blackburn Canyon. This section has an average elevation of 700-850 m and very dense vegetation. From km-point 72.47 to 75.4 we investigated 24 locations and found 38 measurable offset features. The 54 total field and LiDAR-based measurements from this area are listed in Table 1 and can be seen in Figure 11.

The first group of field measurements ranges from 0.5-1.75 m. These offset features are fresh-appearing (apparently young) small-scale, geomorphic features (i.e. drainage rills and bars). The second group of offsets range from 2.3-4.9 m. These offset features are larger-scale, more subdued geomorphic features (i.e. longer-lived drainage gulleys) and appear similar to the other offsets of similar size in Anza Valley and to the southeast. For only a single feature, we find an offset drainage that is roughly double the magnitude of the 2.3-4.9 m offset group at 7.5 m (Fig. 3).

Discussion

Throughout the study area, the field-based and LiDAR-based measurements are in close agreement where both exist for a single feature. In areas of dense vegetation, LiDAR measurements tend to be slightly larger than field measurements. In the field, dense vegetation can prevent a clear and comprehensive view of deformation at and away from the active fault strand, so

that only the near-field deformation is apparent and measurable. In these cases, the filtered LiDAR data affords a perspective of far-field deformation in addition to the deformation at the active fault strand. For geomorphic features with 5 m of offset or less, discrepancies are less than 1 m with only a few exceptions (Fig 12). Where LiDAR measurements are larger than field measurements, discrepancies are typically less than 1 m. Where field measurements are larger than LiDAR measurements, discrepancies are typically less than 0.5 m (Fig. 13).

To estimate slip distribution for recent ruptures, we used the best-preserved and most representative offsets for each section; only offset measurements of confidence seven and greater (good to excellent) were selected for this task. In areas where discrete features are displaced by two or more fault strands, offset measurements are summed and resulting displacement estimates are regarded as minimums. Where only one offset feature is identified in an area of multiple strands, field measurements are regarded as absolute minimums. Individual measurement values are averaged where multiple measurements (field or LiDAR-based) exist for a single feature along strike (i.e. a channel thalweg, NW and SE channel margins). Finally, field and LiDAR-based measurements are averaged for a single offset value per geomorphic feature along strike.

Figures 14 and 15 present two interpreted models of the slip data based on how we choose to interpret a distinct group of small (0.5-1.75 m) offsets in the northwest end of Blackburn Canyon. These small, fresher-looking (interpreted as

younger) offsets are scattered between larger (2.3-4.9 m) offsets on a single strand of the Clark fault. In interpretation A, we attributed these offsets to a smaller rupture event (~15-20 km in length) that is present on only the northwestern Clark fault. This smaller displacement event is superposed on the larger (80+ km rupture) event that we recognized for most of the length of the Clark fault. If the Blackburn Canyon area records evidence for two ruptures during the same timeframe that we interpret only a single event to the south, then the observed surface displacements suggest an earthquake with a *minimum* magnitude of *Mw* 6.5 to M*w* 6.7 through Blackburn Canyon (Fig 14) that post-dates the most recent surface rupture at Anza and to the southeast. By interpreting our observations as a record of two events in Blackburn Canyon, then the penultimate event there corresponds to the most recent event farther south. In this interpretation, the most recent large event at Anza likely extended farther north into the alluvium of Hemet Valley with 2-3 m of displacement rather than 3-4 m – the discrepancy attributed to the 0.5-1.75 m slip in the smaller, more recent event in Blackburn Canyon.

For our alternative interpretation, Scenario B, we attribute all mapped offsets less than 4 m (including the 0.5-1.75 m offsets in Blackburn Canyon) to a single large rupture event (Fig. 15). In this scenario, the rupture may have terminated at the northwest end of Blackburn Canyon, totaling just over ~85 km in length as the displacements drop dramatically in this area (we assume the rupture also continued to the south end of the Clark fault, an additional 10 km

southeast from Lute Ridge). We do not prefer this interpretation because there appear to be two ages of displacements in Blackburn Canyon, with the smaller offsets appearing much fresher (and therefore younger) than the larger ones.

We observe consistent variations in the spatial distribution of these displacements. From Anza to the southeast, measurements taper to less than one meter near the southern termination of the Clark fault in Clark Valley. It should be noted that small offsets in young alluvium are present for an additional ~6-10 km, and scarps are present along the fault for an additional 10-12 km to the southeast of our zero point at Lute Ridge. From Anza to the northwest, displacement measurements taper to 2-3 m in Blackburn Canyon (scenario A), roughly 40 km from the northern termination of the Clark fault, suggesting that the most recent large event continued farther northwest than Blackburn Canyon. Northwest of Blackburn Canyon and Hemet, the Casa Loma fault is geomorphically expressed as the primary surface strand of the SJF zone – essentially a continuation of the Clark fault. This fault zone extends northwest to Mystic Lake where slip steps northeast across the active pull-apart to the Clairemont fault. As there are no significant structural steps between Blackburn Canyon and Mystic Lake, it is plausible that the largest ruptures identified along the Clark fault continued as far north as Mystic Lake (an additional 40 km), or farther.

The probable moment magnitude of recent events along the Clark fault can be estimated using $Mo = \mu As$ (Brune, 1968) along with $Mw = 0.667 \log Mo -$

10.7 (Hanks and Kanamori, 1979), where *Mo* is the seismic moment, μ is rigidity (3.1×10^{11} dyne/cm^2), *A* is the area of the rupture, and *s* is the average displacement in the event. When calculating seismic moment and magnitude, it is assumed that most large earthquakes rupture to the maximum depth of microseismicity on the fault (Sibson, 1984). The depth of seismicity along strike of the entire SJF system varies not only from fault to fault, but also for different sections along a single strand.

For the Clark fault, we separate the fault into four different sections based on the depth of seismicity as assessed by Sanders (1989). For the Clairemont fault segment and the Clark-Casa Loma fault southward to the Anza gap, the seismogenic depth is estimated to be ~17 km. Within the 20 km stretch deemed the Anza seismicity gap, there is little to no microseismicity; however, from the scattered data, depth is estimated to be ~20 km. South of the Anza gap and into southern Clark Valley, seismicity shallows again to an average depth of ~17 km. From Clark Valley to the southern termination of the fault just south of the Santa Rosa Mountains, the depth of microseismicity is ~14 km (Sanders, 1989).

Using the two scenarios, we estimate the size of the earthquakes that likely generated the observed offsets. The average right-lateral displacement in the most recent event in both models is on the order of 2.7-2.9 m, with maximum slip near Anza at 3.9 m (Fig. 14). With a likely minimum rupture length of ~85 km in model B (south end of fault in the San Filipe Hills northwest to the northern end of Blackburn Canyon) and a minimum average slip of 2.7 m, this suggests a

minimum moment release of ~10^{27} dyne cm, which corresponds to a M*w* 7.3 earthquake. Double-event offsets resolved for the same section of the Clark fault show an average of ~5.5 m of total right-lateral displacement -- about twice as much average displacement. Maximum slip values in the penultimate event are close to 3 m near Anza. These data suggest that the penultimate event was similar in size to the MRE**.** The third event is also similar in size, with cumulative displacement of 9-10 m through Anza for the past three events. For model A, where we recognize the likely occurrence of a younger, short, ~20 km section of rupture of the fault (with an average of 1.25 m of right-lateral displacement) in Blackburn Canyon, we estimate that the minimum magnitude required to have produced this rupture is M*w* 6.7, as there may have also been blind rupture farther along the fault.

Historical and Paleoseismic Events

There are several historical and pre-historical earthquakes that could be attributed to the observed offsets along the Clark fault. Here, we explore which of the historical events may have contributed to the offsets, and discuss the paleoseismic record documented for the past several thousand years at Hog Lake near Anza, close to where the maximum displacements are observed.

The SJF zone is historically the most seismically active fault zone in southern California with 10 earthquakes greater than ~M6 since 1890 (Sanders and Kanamori, 1984) (Fig. 1). Four of these (1899, 1918, 1937, 1954) are well-

documented and have been attributed to the Clark or Casa Loma strands of the SJF zone, with the 1937 event likely occurring between the Clark and Buck Ridge faults (Doser, 1990; Sanders et al., 1986). Toppozada et al. (1981) tentatively place two more historic events on the Clark fault, 1890 and 1892, but these were recorded only at distant localities (Los Angeles, San Diego, Yuma) and could have occurred anywhere in the southern San Andreas system. Furthermore, they were probably no larger than about M*w* 6.5 (Toppazada et al., 1981), so neither is likely to have cause the large displacements observed for the most recent rupture along the Clark fault (Fig 16 A and B).

The 1899 and 1918 events are inferred to have occurred on the Clark–Casa Loma segment of the SJF zone near Hemet, California. The 1899 "Christmas Day" M6.4 (Ellsworth, 1990) produced a relatively circular isoseismic pattern of felt effects (Toppazada et al., 1981) (Fig.16 C). Rasmussen (1981) places this event on the Casa Loma fault, which is the northwest extension of the Clark fault and the southwest-bounding fault of the Hemet step-over.

The larger, April 21, 1918 event (Ellsworth, 1990, estimates this event at *Mw* 6.9) produced an elongated isoseismic pattern of felt effects and damage (Toppazada et al., 1981), indicating a larger source dimension and making it the more likely of the two to have produced a surface rupture (Fig. 16 D). Doser (1992) places this event on the Clairemont fault – the northeast-bounding fault of the Hemet step-over, although the relatively high intensities associated with this

earthquake near Anza and Terwilleger Valley suggest that the source was actually farther southeast on the Clark fault.

Though both of these earthquakes produced surface cracking and were potentially large enough to have produced a surface rupture, no co-seismic surface ruptures were documented at the time (Claypole, 1900; Townley, 1918; Rolfe and Strong, 1918). Rolfe and Strong (1918) reported that they did not see any evidence of surface ruptures northwest of Blackburn Canyon, but their reconnaissance report in 1918 clearly states that, for various reasons, there was no trip into Blackburn Canyon itself. Instead, the explorers took Bautista Road around this area and reported neither a rupture at Hog Lake nor any points farther south (Rolfe and Strong, 1918), although there was abundant evidence of very strong ground shaking.

We attribute the smallest displacements found in Blackburn Canyon to the April 21, 1918 earthquake. This is specifically described as an area that was not checked for surface rupture, and the small offsets in Blackburn Canyon appear young and fresh. Furthermore, the 15-20 km of surface displacements that we describe are consistent with the 1918 earthquake, although the total subsurface rupture length was probably longer than we see evidence for in the geomorphology.

Of the other historic events on the southern Clark fault, both the 1937 and 1954 earthquakes were too small to have produced surface ruptures. Thus, since at least 1890, there have been no historical earthquakes that could have

produced the most recent rupture within the Anza seismicity gap or along most of the southern Clark fault.

The Hog Lake paleoseismic site (Rockwell et al., 2006) falls within the "Anza Seismicity Gap" (Sanders et al., 1997), the middle section of the Clark fault where microseismicity extends to nearly 20 km depth on the edges of the gap (Sanders and Kanamori, 1984). The stratigraphy at Hog Lake records the timing of the past 18 surface ruptures over the past 3800 years with an average return period of about 210-230 years (Rockwell et al., 2006). Of interest to this study are the past several events, as some or all of these may be responsible for the observed displacements along the Clark fault.

At Hog Lake, the youngest event is radiocarbon dated at ca. 1790, potentially placing the last surface rupture in the Historic period. A clear mismatch in near-surface stratigraphic units suggests that displacement was significant (Rockwell et al., 2006). We attribute the 3-4 m displacements in the Anza region to the most recent surface rupture event identified (ca. 1790) at Hog Lake. This event cannot correspond to the 1918 earthquake, as people went to Hog Lake and reported the absence of surface rupture there (Rolfe and Strong, 1918). Of other early-historic large earthquakes, the November 22, 1800 event fits well with a large rupture along the Clark fault. This poorly located event caused extensive damage (MMI VII) at San Diego and San Juan Capistrano missions – the only two locations it was recorded.

To better constrain the magnitude and potential location of the 1800 earthquake, we examined the relationships between enclosed areas of various MMI contours and associated earthquake magnitudes (Toppozada, 1975; Toppozada, 1981). We estimate the area of an ellipse centered on the Clark fault near Anza with both the San Diego and San Juan Capistrano Missions located on or near the fringe of the MMI VII contour (Fig. 16 E). Initial estimates place the earthquake magnitude at ~M7.8 – substantially larger than what our field data indicate, assuming that the intensity VII values are correct. However, descriptions by Toppozada et al. (1981) of MMI VI and VII for cracked walls are very similar, and combined with the potentially very poor adobe construction standards of 1800, we do not think it unreasonable to assume a MMI VI to VII, or VI+ (instead of VII) for the two missions. Placing the San Diego and San Juan Capistrano missions in the MMI VI+ range yields magnitude estimates of M*w* 7.2 to M*w* 7.6, more consistent with our field-observed slip distributions (Fig. 16 F)

In summary, our data suggest that the November 22, 1800 earthquake occurred on the Clark strand of the SJF and produced the offset geomorphology we observe through the Anza seismicity gap and along most of the Clark fault. If correct, then it has been about 210 years since the last major rupture, which is also the estimated average recurrence interval determined at Hog Lake.

For earlier events dated at Hog Lake, we tentatively attribute the double and triple-event displacements recognized from the geomorphology to the ca. 1551 and ca. 1380 earthquakes recognized in the stratigraphy at Hog Lake

(Rockwell et al., 2006). If correct, there has been 9-10 m of slip along the central SJF during the past 630 years or so, consistent with a slip rate of about 15 mm/yr.

Our preferred slip distribution interpretation (scenario A) involves multiple surface rupture events that have occurred recently enough for their offset features to remain preserved. We suggest a similar rupture pattern to that of the Imperial Valley earthquakes of 1940 and 1979 in which Sieh (1996) proposes a "patch" model for slip distribution. During the 1940 M7.1 Imperial Valley earthquake, up to 6 m of slip was measured near the central section of the fault after nucleating with less than a meter of slip along the northern third of the fault. The M6.6 earthquake of 1979 ruptured only the northern 30 km of the fault with nearly identical slip distribution for that segment as in the earthquake of 1940. From this observation, Sieh (1996) inferred that smaller earthquakes nucleate in segments adjacent to stronger sections of the fault, where larger displacements are recorded.

We propose the following scenario for recent ruptures of the Clark Fault. Similar to the Imperial Valley earthquake of 1940, the 1800 earthquake may have occurred on the Clark Fault, rupturing the entire 120-km length in a M*w* 7.2 to M*w* 7.5 earthquake. In the southeast near San Felipe hills, offsets are below one meter and increase towards maximum offset values (nearly 4 m) through the Anza seismicity gap and Hog Lake. Slip decreases dramatically to the north of Anza, but still continues for the entire length of the fault through Blackburn

Canyon and into San Jacinto Valley near Hemet. Similar to the 1979 Imperial Valley quake, the M*w* 6.9 1918 event ruptured a relatively short segment (~15-20 km) of the fault through Blackburn Canyon as a consequence, in part, due to the lower displacements in this area during the 1800 event.

Inference on the Recurrence Interval

The slip rate at Anza has been determined for a ~4.3 ka channel that is offset ~75 m across a section of the fault where displacement is localized (Blisniuk et al., 2010 in prep.). The resulting rate of about 16.7 ± 4.3 mm/yr can be used with the average displacements observed in the geomorphology to estimate an average repeat time. For this calculation, we use 3.5 ± 0.5 m of slip per event. Assuming that all events have displacement at Anza in this range, these observations suggest a recurrence interval of $210^{+112}/_{-67}$ years, which is similar to the 210-230 year recurrence interval determined from trenching (Rockwell et al., 2006). All available data indicate that recurrence, displacement, and slip rate are consistent over the time scale of several thousand years for the Clark strand of the SJF.

Conclusion

We mapped small geomorphic offsets for 80 km of the Clark fault from the southeast end of Clark Valley (east of Borrego Springs) northwest to the mouth of

Blackburn Canyon (near Hemet) using raw and filtered B4 LiDAR data, aerial photographs, and field techniques. Estimates made from offset features for these 80 km suggest that average displacement for the most recent event identified at Hog Lake is on the order of 2.5-2.9 m, and, depending on the preferred model, maximum slip near Anza is estimated to be about 3.9 m. We tentatively attribute these offsets to the November 22, 1800 earthquake that produced damage at the San Juan Capistrano and San Diego missions.

Displacement in the penultimate large event was resolved for the same 80 km section by assuming that larger offset clusters can be attributed to displacement in the past two or more events. Based on this assumption, the average amount of right-lateral slip is estimated at ~5.5 m for the past two events, which suggests a similar estimate for average displacement in the penultimate event -- about 2.7 m. Similarly, using the maximum values near Anza, we estimate that the penultimate event produced about 3 m of displacement in the “seismicity gap”, so the penultimate event (assumed to be ca. 1550 from paleoseismic trenching) was very similar to the MRE based on this value alone. Using the average displacement for each event, they are nearly identical.

The third event is also similar in size, with cumulative displacement of 9-10 m through Anza for the past three events. Data elsewhere along the fault for this event are sparse, but are consistent with the rupture pattern from the two most recent earthquakes. Thus, these geomorphic observations argue for fairly

characteristic slip along the Clark fault for at least the past three events. We also recognize the likely rupture from the April 21, 1918 earthquake, which broke a short 15-20 km section of the fault (with an average of 1.25 m of right-lateral displacement) in Blackburn Canyon, apparently due to lower displacement in that area in the ca. 1800 event. Thus, the Clark fault has not behaved in a strictly characteristic fashion, although these observations are still consistent with the slip-patch model of Sieh (1996).

To the northwest of Blackburn Canyon, the flat bottom of the San Jacinto Valley, commercial development, and recent sedimentation make additional measurements with LiDAR data and field techniques impossible. To the southeast, offsets in very young alluvium are present for an additional ~5 km, and scarps are present along the fault for an additional 10-12 km to the southeast of our zero point. Thus, although the minimum rupture length for the earthquakes inferred from the observed offsets is probably on the order of 85-90 km, it is possible that some or all of the larger displacements correspond to earthquakes with rupture lengths of 100-120 km if they involved both the Clark and Casa Loma fault strands. Such an earthquake could have devastating effects on the urbanized Hemet region, as well as the densely populated Riverside and San Bernardino areas to the northwest.

Data and Resources

The B4 dataset was acquired in May 2005 as a pre-earthquake survey of the SAF and SJF zones in southern California. For more information about the B4 project, please visit <http://www.earthsciences.osu.edu/b4/Site/Welcome.html>. The B4 LiDAR dataset is available in many formats via <http://www.opentopography.org> for neotectonic and paleoseismic research.

References

Bennett, R. A., A. M. Friedrich, and K. P. Furlong (2004). Codependent histories of the San Andreas and San Jacinto fault zones from inversion of fault displacement rates, *Geology*, **32**, no. 11, 961-964.

Blisniuk, K. L., T. K. Rockwell, L. A. Owen, M. Oskin, C. Lippincott, M. W. Caffee, and J. Dortch (in review). Late Quaternary slip rate gradient defined using high-resolution topography and ^{10}Be dating of offset landforms on the southern San Jacinto Fault zone, California, *J. Geophys. Res.*.

Brune, J. N. (1968). Seismic moment, seisimicity, and rate of slip along major fault zones, *J. Geophys. Res.*, **73**, 777-784.

Claypole, E. W. (1900). The earthquake at San Jacinto, December 25, 1899, *Am. Geologist*, **25**, 106-108.

DeMets, C., and T. H. Dixon (1999). New kinematic models for Pacific-North America motion from 3 Ma to present, Evidence for steady state motion and biases in the NUVEL-1A model, *Geophys. Res. Lett.*, ***26***, 1921-1924, doi 10.1029/1999GL900405.

Dorsey, R. J. (2002). Stratigraphic record of Pleistocene initiation and slip on the Coyote Creek fault, lower Coyote Creek, southern California, in *Contributions to crustal evolution of the southwestern United States* A. Barth (Editor), *Geol. Soc. Am. Sp. Ppr.* 365, Boulder, Colorado, *Geol. Soc. Am.*, 251-269.

Doser, D. I. (1990). Source Characteristics of earthquakes along the southern San Jacinto and Imperial fault zones (1937 to 1954), *Bull. Seismol. Soc. Am.*, **80**, no. 5, 1099-1117.

Doser, D. I. (1992). Historic earthquakes (1918 to 1923) and an assessment of source parameters along the San Jacinto fault system, *Bull. Seismol. Soc. Am.*, **70**, 185-201.

Ellsworth, W. L. (1990). Earthquake history, 1769-1989, in *The San Andreas Fault System, California* R. E. Wallace (Editor), *U.S. Geol. Surv. Pro. Ppr. 1515*, 153-187.

Evans, J. S., and A. T. Hudak (2007). A multiscale curvature algorithm for classifying discrete return LiDAR in forested environments, *IEEE Trans. on Geoscience and Remote Sensing*, **45**, no. 4,1029-1038.

Fialko, Y. (2006). Interseismic strain accumulation and the earthquake potential on the southern San Andreas fault system, *Nature*, **441**, no. 7096, 968-971.

Hanks, T. C., and H. Kanamori (1979). A moment-magnitude scale, *J. Geophys. Res.*, **84,** 2348-2350.

Janecke, S. U., S. M. Kirby, V. E. Langenhiem, B. A. Housen, R. J. Dorsey, R. E. Crippen, and R. G. Blom (2004). Kinematics and evolution of the San Jacinto fault zone in the Salton Trough: progress report from the San Felipe Hills area, *Geol. Soc. Am. Abs. Prog.*, **36**, no. 5, 317.

Kondo, H., Y. Awata, O. Emre, A. Dogan, S. Özalp, F. Tokay, C. Yildirim, T.

Yoshioka, and K. Okumura (2005). Slip distribution, fault geometry and fault segmentation of the 1944 Bolu-Gerede earthquake rupture, North Anatolian fault, Turkey, *Bull. Seismol. Soc. Am.*, **95**, no. 4, 1234-1249.

Lindvall, S. C., T. K. Rockwell, and K. W. Hudnut (1989). Evidence for prehistoric earthquakes on the Superstition Hills fault from offset geomorphic features, *Bull. Seismol. Soc. Am.*, **79**, no. 2, 342-361.

Matti, J. C., D. M. Morton, and B. F. Cox (1992). The San Andreas fault system in the vicinity of the central Transverse Ranges province, Southern California, *U.S. Geol. Surv. Open-File Report*, OF 92-0354.

Merifield, P. M., T. K. Rockwell, and C. C. Loughman (1991). A slip rate based on trenching studies, San Jacinto fault zone near Anza, California, in *Eng. Geo. Geotech. Eng.* J. P. McCalpin (Editor), 1-12.

McGill, S. F., and C. M. Rubin (1999). Surficial slip distribution on the central Emerson fault during the June 28, 1992, Landers earthquake, California, *J. Geophys. Res.*, **104**, no. B3, 4811-4833.

McGill, S. F., and K. E. Sieh (1991). Surficial offsets on the central and eastern Garlock fault associated with prehistoric earthquakes, *J. Geophys. Res.*, **96**, no. B13, 21,597-21,621.

Morton, D. M., and J. C. Matti (1993). Extension and contraction within an evolving divergent strike-slip fault complex: The San Andreas and San Jacinto fault zones at their convergence in Southern California, in *The San Andreas fault system: Displacement, palinspastic reconstruction, and*

geologic evolution R. E. Powell et al. (Editors), Boulder, Colorado, *Geological Society of America Memoir*, 178, 217-230.

Rasmussen, G. S. (1981). Nature of surface rupture and recurrence interval, Casa Loma fault, in *Geology of the San Jacinto Mountains, South Coast Geological Society Annual Field Trip Guidebook 9*, *South Coast Geol. Soc.*, Santa Ana, California, 48-54.

Rockwell, T. K. (1990). Holocene activity of the Elsinore fault in the Coyote Mountains, Southern California, in *F.O.P. Guidebook and Volume on Western Salton Trough- Soils and Neotectonics*, 30-42.

Rockwell, T. K., and C. T. Pinault (1986). Holocene slip events on the southern Elsinore fault, Coyote Mountains, Southern California, in *Guidebook and Volume on Neotectonics and Faulting in Southern California, Cordilleran Section* P. Ehlig (Editor), *Geol. Soc. Am.*, 193-196.

Rockwell, T. K., C. Loughman, and P. Merifield (1990). Late Quaternary rate of slip along the San Jacinto fault zone near Anza, Southern California, *J. Geophys. Res.*, **95**, no. B6, 8593-8605.

Rockwell, T. K., G. Seitz, T. Dawson, and J. Young (2006). The long record of San Jacinto fault paleoearthquakes at Hog Lake: Implications for regional patterns of strain release in the southern San Andreas fault system, *Seismol. Res. Lett.*, **77**, no. 2, 270.

Rolfe, F., and A. M. Strong (1918). The earthquake of April 21, 1918, in the San Jacinto Mountains, *Bull. Seismol. Soc. Am.*, **8**, 63-67.

Sanders, C. O. (1989). Fault segmentation and earthquake occurrence in the strike-slip San Jacinto fault zone, California, in *Proceedings of Conference XLV, Workshop on fault segmentation and controls of rupture initiation and termination* D. P. Schwartz and R. H. Sibson (Editors), *U.S. Geol. Surv. Open-File Report*, OF 89-0315, 324-349.

Sanders, C. O., and H. Kanamori (1984). A seismotectonic analysis of the Anza Seismic Gap, San Jacinto fault zone, Southern California, *J. Geophys. Res.*, **89**, no. B7, 5873-5890.

Sanders, C. O., and H. Magistrale (1997). Segmentation of the northern San Jacinto fault zone, Southern California, *J. Geophys. Res.*, **102**, no. B12, 27,453- 27,467.

Sanders, C. O., H. Magistrale, and H. Kanamori (1986). Rupture patters and preshocks of large earthquakes in the southern San Jacinto fault zone, *Bull. Seismol. Soc. Am.*, **76**, no. 5, 1187-1206.

Sharp, R. V. (1967). San Jacinto fault zone in the Peninsular Ranges of Southern California, *Geol. Soc. Am. Bull.*, **78**, 705-730.

Sharp, R. V. (1972). Map showing recently active breaks along the San Jacinto fault zone between the San Bernardino area and Borrego Valley, California, scale 1:24,000, *U.S. Geol. Surv. Misc. Geologic Investigations Map*, I-675.

Sharp, R. V. (1981). Variable rates of Late Quaternary strike slip on the San Jacinto fault zone, Southern California, *J. Geophys. Res.*, **86**, no. B3,

1754-1762.

Sibson, R. H. (1984). Roughness at the base of the seismogenic zone: Contributing factors, *J. Geophys. Res.*, **89**, 5791-5799.

Sieh, K. E. (1978). Slip along the San Andreas fault associated with the great 1857 earthquake, *Bull. Seismol. Soc. Am.*, **68**, no. 5, 1421-1448.

Sieh, K. E. (1996). The repetition of large-earthquake ruptures, *Proceedings of the National Academy of Sciences of the United States of America*, **93**, 3764-3771.

Toppozada, T. R. (1975). Earthquake magnitude as a function of intensity data in California and western Nevada, *Bull. Seismol. Soc. Am.*, **65**, no. 5, 1222-1238.

Toppozada, T. R., C. B. Real, and D. L. Parke (1981). Preparation of isoseismal maps and summaries of reported effects for pre-1900 California earthquakes, *Open File Report 81-11 SAC, California Division of Mines and Geology*, Sacramento, California.

Townley, S.D. (1918). The San Jacinto earthquake of 1918, *Bull. Seismol. Soc. Am.*, **8**, 45-63.

Wells, D. L., and K. J. Coppersmith (1994). New empirical relationships among magnitude, rupture length, rupture width, rupture area, and surface displacement, *Bull. Seismol. Soc. Am.*, **84**, no. 4, 974-1002.

Zielke, O., J. R. Arrowsmith, L. G. Ludwig, S. O. Akciz (2010). Slip in the 1857 and earlier large earthquakes along the Carizzo Plain, San Andreas Fault, *Science*, **327**, no. 5969, 1119-1122.

Authors' Affiliations, Addresses

J. B. Salisbury[1]

T. K. Rockwell[1]

T. J. Middleton[1]

K. W. Hudnut[2]

[1]Department of Geological Sciences, MC-1020

5500 Campanile Drive

San Diego State University

San Diego, CA 92182

USA

[2]U.S. Geological Survey

525 South Wilson Avenue

Pasadena, CA 91106

USA

Table 1

Lute Ridge displacement data (LR)

						Field			LiDAR (QTM)		
#	Location	Feature	Longitude	Latitude	Distance along fault	Meters	±	Confidence	Meters	±	Confidence
1	LR-1	TH	575130	3685868	1.65	0.8	0.1	6.5			
2	LR-2	TH	575092	3685891	1.7	0.9	0.2	7			
3	LR-3	TH	574789	3686002	2	1	0.2	7			
4	LR-4	TH	574498	3686195	2.35	1.3	0.3	6.75			
5	LR-5	TH	574490	3686201	2.36	1.5	0.3	7	1.25	0.2	6.5
6	LR-6	TH	574486	3686208	2.36	3.9	0.6	6			
7		TH				1.1	0.2	6			
8	LR-7	TH	574456	3686220	2.4	1.3	0.4	6	1.1	0.3	6.5
9	LR-8	TH	574435	3686239	2.42	1.4	0.3	7.25	1.2	0.3	6.5
10	LR-9	TH	574428	3686230	2.42	1.5	0.6		1.4	0.4	7
11	LR-10	TH	574390	3686263	2.47	2.8	0.4	8.5	2.9	0.3	7.5
12		SE				2.9	0.3	8.5	2.7	0.2	7.5
13		NW							2.8	0.3	7.5
14	LR-11	FA	574390	3686263	2.47	1.1	0.3	6.5			
15	LR-12	TH	574368	3686269	2.5	2.5	0.4	7	2.6	0.4	7
16	LR-13	TH	574258	3686332	2.62	1.5	0.4	7.5	1.5	0.2	7.5
17		SE				1.4	0.5	7.5	1.4	0.3	7.5
18	LR-14	TH	574103	3686407	2.79	1.4	0.2	6			
19	LR-15	TH	573905	3686536	3.03	1.4	0.3	6.5			
20	LR-16	TH	573905	3686536	3.03	1.5	0.4	7.5	1.1	0.4	7.5
21	LR-17	TH	573905	3686536	3.03	2.9	0.3	8	2.9	0.3	7.5
22		SE				2.7	0.5	8	2.7	0.4	7.5

Rockhouse Ridge displacement data (RR)

						Field			LiDAR (QTM)		
#	Location	Feature	Longitude	Latitude	Distance along fault	Meters	±	Confidence	Meters	±	Confidence
1	RR-1	TH	561085	3695356	18.58	2.3	0.7	5.75	2.2	0.5	5.5
2	RR-2	TH	560961	3695425	18.73	1.9	0.4	6.75	2.3	0.4	6.5
3	RR-3	TH	560613	3695583	19.1	6	0.4	6.25			
4		TH			19.1	2.7	0.7	5.5			
5	RR-4	TH	559754	3696113	20.11	2.2	0.5	7.5	2.1	0.3	7.5

Rockhouse Canyon displacement data (RC)

						Field			LiDAR (QTM)		
#	Location	Feature	Longitude	Latitude	Distance along fault	Meters	±	Confidence	Meters	±	Confidence
1	RH-1	BC	558158	3696972	21.91				22.1	1.5	6.5
2	RH-2	BC	558112	3697001	21.97				21.9	1.6	6.5
3		BC				5.5	0.5	7.5	5.6	0.4	7.5
4	RH-3	TH	558104	3697005	21.98				2.6	0.3	7
5		TH							5.2	0.7	6.5
6	RH-4	BC	558095	3697010	21.99	2.3	0.4	7	2.5	0.3	7
7	RH-5	SE	557954	3697119	22.16	2.7	0.3	7.5	3.1	0.4	7.5
8		TH							2.7	0.5	7.5

Jackass Ridge displacement data (JAR)

						Field			LiDAR (QTM)			Aerial Photography	
#	Location	Feature	Longitude	Latitude	Distance along fault	Meters	±	Confidence	Meters	±	Confidence	Meters	±
1	JAR-1	TH	553551	3699798	27.31	2.6	0.4	9	2.5	0.5	8	2.5	0.5
2		NW			27.31	2.9	0.5	9	3.1	0.5	8	3	0.5
3	JAR-2	TH	553491	3699848	27.39	1.6	0.3	7.5	1.8	0.4	8	2	0.5
4		NW										1	0.5
5	JAR-3L	SE	553479	3699851	27.4	3.7	0.5	6.5				3.5	0.5
6	U	SE							2.3	0.4	6.5	1.5	0.5
7	T	SE										5	0.5
8	L	NW				3.4	0.7	5.5				4	0.5
9	U	NW				1.9	0.4	6				1	0.5
10	T	NW				5.3	0.6					5	0.5
11	JAR-4	SE	553437	3699874	27.45	2.2	0.3	6	2.2	0.8	6.5	2	0.5
12		NW							2.8	0.4	6.5	3.5	0.5
13	JAR-5	SE	553375	3699925	27.53	2.1	0.6	9.5	2.8	0.3	8.5	2.5	0.5
14		NW				2	0.4		2.5	0.4	8.5	1.75	0.5
15	JAR-6	SE	553318	3699961	27.6	8	0.6	7	7.5	1	7	5.5	0.5
16		SE				2.7	0.5	8.5	2.5	0.5	7		
17		NW				2.9	0.5	8				3.5	0.5
18	JAR-7L	NW	553258	3699967	27.65							1.5	0.5
19	U	NW				2.3	0.6	7	1.9	0.3	7	0.75	0.5
20	T	NW				2.3	0.6					2.25	0.5
21	L	SE	553245	3699975	27.67	2.3	0.4	7				1.75-2	0.5
22	U	SE				1.6	0.4	8				0.5	0.5
23	T	SE				3.9	0.4					2.5	0.5
24	L	NW										2.75	0.5
25	U	NW										1	0.5
26	T	NW										3.75	0.5
27	JAR-9L	RN	553227	3700004	27.7	1	0.2	7.5				1.5	0.5
28	U	RN				2.1	0.4	7.5				1.0-.25	0.5
29	T	RN				3.1	0.3					2.75	0.5
30	JAR-10	SE	553160	3700050	27.78	6.2	1	6	6.3	0.5	7.5	4	0.5
31		TH				2.4	0.4	7.5	2.9	0.6	7.5	3	0.5
32		NW										2.0-.5	0.5
33	JAR-11	SE	553133	3700059	27.81	2.6	0.4	7.5	2.65	0.4	7.5	2.75	0.5
34		TH							2.7	0.3	7.5		
35		NW							2.7	0.5	7.5	2.5	0.5
36	JAR-12	SE	553111	3700080	27.84	2.5	0.4	6.5	2.6	0.4	6.5	2.75	0.5
37		RN				3.3	0.6	7.5	3.5	0.6	7.5		
38		NW							2.8	0.4	7.5	2.75	0.5
39	JAR-13	TH	553081	3700082	27.86							3	0.5
40	JAR-14	SE	553081	3700082	27.86							2.25	0.5
41		NW							2.25	0.6	6	2.75	0.5
42	JAR-15L	TH	553053	3700114	27.9							2	0.5
43	U	TH										0.75-1	0.5
44	T	TH							3.2	0.5	7	2.75	0.5
45	JAR-16	NW	553015	3700153	27.96	1.8	0.5	<5	3.1	0.6	7	2.5	0.5
46	JAR-17	TH	552965	3700164	28	2.5	0.6	5	2.8	0.3	7	1.5	0.5
47	JAR-18U	NW	552942	3700173	28.03							1.5	0.5
48	L	NW							1.3	0.4	5.5	1.5	0.5
49	T	NW										3	0.5
50	JAR-19	SE	552942	3700178	28.03	1.5	0.4		2.9	0.6	6	3.5	0.5
51	JAR-A	SE	552917	3700192	28.06				3.5	0.6	6		
52		TH							2.6	0.3	7.5		
53		NW							2.7	0.3	7		
54	JAR-B	TH	552911	3700194	28.07				2	0.4	6		
55	JAR-20	SE	552798	3700271	28.2	2.5	0.4	9.5	2.3	0.4	8		
56		TH				2.2	0.3	9.5	2.4	0.3	8		
57		NW				1.9	0.3	9.5	2.2	0.4	8		
58	JAR-21L	SE	552712	3700318	28.3	1.7	0.3	5.5					
59	U	TH				1.5	0.4	5.5					
60	L	TH				2.2	0.4	7					
61	T	TH				3.7	0.4						
62	JAR-C U	SE	552736	3700307	28.27				2.4	0.3	6		
63	T	SE							5.4	0.9	5		
64	JAR-D	SE	552694	3700321	28.32				2.9	0.4	6.5		
65		TH							2.7	0.3	6.5		
66		NW							3.2	0.5	5.5		
67	JAR 22	SE	552589	3700387	28.44	7	1	6.5	7.5	0.75	6		

Dry Wash-Jackass Ridge displacement data (DW-JAR)

#	Location	Feature	Longitude	Latitude	Distance along fault	Field Meters	Field ±	Field Confidence	LiDAR (QTM) Meters	LiDAR (QTM) ±	LiDAR (QTM) Confidence
68	DW-JAR-1	BC	552153	3700704	28.98	2.7	0.5	7.5	2.6	0.4	7
69	DW-JAR-2	TH	552139	3700708	28.99	2.5	0.3	6	2.3	0.4	7
70	DW-JAR-3	SE	552123	3700715	29.01	2.8	0.5	6.5	2.9	0.3	7.5
71		TH				2.5	0.4	7	2.6	0.3	7.5
72	DW-JAR-4	NW	552091	3700734	29.05				2.5	0.4	7.5
73	DW-JAR-5	BC							17	1	8

Dry Wash displacement data (DW)

#	Location	Feature	Longitude	Latitude	Distance along fault	Field Meters	Field ±	Field Confidence	LiDAR (QTM) Meters	LiDAR (QTM) ±	LiDAR (QTM) Confidence
1	DW-1	TH	551510	3701100	29.73	12.5	1.5	4.5	16	2	4
2	DW-2	SE	551483	3701115	29.77	1.5	0.4	6			
3		TH			29.77	1.7	0.4				
4	DW-3	BC	551418	3701157	29.84	2.9	0.4	8.5	2.8	0.6	7.5
5		TH			29.84	2.5	0.6	7.5	2.6	0.5	7
6		SE							8.5	0.75	7
7	DW-A	TH	551307	3701207	29.96				2.5	0.4	7
8	DW-4	NW	551149	3701297	30.14	2.7	0.4	6.5	2.8	0.5	<5
9	DW-5	NW	551054	3701346	30.25	2.5	0.5	6	3.2	0.6	5
10	DW-B	BW	551013	3701362	30.29				6.5	1	5
11	DW-C	SE	550945	3701359	30.35				2.6	0.3	6.5
12	DW-6	NW	550925	3701399	30.39	3.1	0.6	6.5	3.2	0.3	7.5
13		NW							6.1	0.5	7
14	DW-7	NW	550800	3701463	30.53	2.9	0.7	6	2.4	0.4	7.5
15		NW							5.8	0.6	6
16		TH							2.5	0.3	7.5
17	DW-8	NW	550762	3701494	30.58	3.1	0.6	7	2.8	0.4	7.5
18		NW							9.4	0.6	6.5
19		TH							2.9	0.5	6
20	DW-9	RN	550606	3701600	30.76	2.5	0.5	7	3.1	0.6	5.5
21	DW-10	SE	550560	3701606	30.81	2.8	0.3	7			
22		TH			30.81	2.5	0.4	7			
23	DW-11	NW	550367	3701892	31.12	3.1	0.4	7.75	2.8	0.3	
24		TH			31.12	2.6	0.4	7.75	2.6	0.4	
25		SE			31.12	2.7	0.4	7.75	2.6	0.3	
26	DW-D	NW	550382	3701879	31.1				6.5	0.75	6
27	DW-12	NW	549605	3702547	32.12	3.5	0.7	7.5	6.3	0.75	6
28		TH							2.5	0.6	6
29	DW-13	TH	549413	3702580	32.3	4.6	0.4	6.5			
30	DW-14	SE	549312	3702612	32.4	2.1	0.5	6			
31		TH			32.4	2.5	0.5	6.5	2.8	0.6	6.5
32	DW-15	NW	549212	3702662	32.51	4.9	0.6	6	4.3	0.5	6.5
33		BC			32.51	3.1	0.5	5.5			
34		TH							3.2	0.4	7
35	DW-16	NW	549179	3702687	32.55	3.3	0.5	7.5	2.6	0.6	7
36		TH			32.55	3.1	0.4	7.5	2.7	0.3	7.5
37	DW-17	NW	549161	3702697	32.57	3.1	0.4	6.5	3.9	0.6	6
38		TH							2.9	0.5	7.5
39	DW-18	TH	549104	3702763	32.66	2.7	0.5	7.5	3.2	0.3	7.5
40		TH							5.9	0.6	6
41		NW				2.9	0.4	7.5	2.9	0.3	7.5
42	DW-E	NW	549062	3702792	32.67				2.7	0.4	7
43		TH			32.67				2.8	0.6	6

Horse Canyon and White Wash displacement data (HC-WW)

#	Location	Feature	Longitude	Latitude	Distance along fault	Field Meters	Field ±	Field Confidence	LiDAR (QTM) Meters	LiDAR (QTM) ±	LiDAR (QTM) Confidence
1	WW-1	SE	544649	3705282	37.77	2.6	0.3	6			
2		NW				2.5	0.4	6			
3	WW-2	TH	544334	3705524	38.16	3	0.3	6.5			
4	WW-3	SE	544300	3705554	38.21	2.4	0.3	6.5	3	0.4	7
5		NW				2.3	0.3	6.5	3.1	0.5	7
6		TH							3.2	0.5	7
7	WW-4	BC				2.3	0.5	6.5			
8	WW-A	TH	544250	3705583	38.26				3	0.5	6.5
9	WW-5U	NW	543561	3706384	39.28	1.9	0.3	7			
10	L	NW				1.1	0.5	6			
11	T	NW				3	0.4	6.5			
12	U	TH				1.8	0.5	6.5			
13	L	TH				1.3	0.5	6			
14	U	TH				3.1	0.5	6.25			
15	U	SE				2	0.3	7			
16	L	SE				1.2	0.4	6.5			
17	T	SE				3.2	0.4	6.75			
18	WW-B	SE	543634	3706282	39.16				3.2	0.5	7
19		TH							3.1	0.4	7
20	WW-6	TH	543394	3706519	39.49	2.2	0.4	7	2.4	0.6	7
21		NW				2.7	0.5	7	2.6	0.4	7
22		SE				2.6	0.4	7	2.7	0.4	7
23	WW-7	SE	543388	3706531	39.5	2.9	0.3	7.5	3.4	0.3	7.5
24		TH							3.2	0.4	7.5
25		TH							6.5	0.7	7
26	WW-8	TH	543279	3706681	39.68	3.1	0.5	7.5	3.2	0.5	7.5
27		SE				2.9	0.4	7.5	2.9	0.6	7
28		NW				3.2	0.6	7	3.1	0.3	7.5
29		TH	543275	3706694	39.69				5.9	0.6	7
30	WW-9	SE	543112	3706808	39.89	2.1	0.6	5.5			
31	WW-10	TH	543098	3706831	39.91				6.2	0.8	5.5
32		NW				3	0.5	7.5	3.2	0.4	7
33		TH				3.1	0.5	7.5			
34		SE				3.3	0.6	7			
35	WW-11	SE	542932	3706975	40.13	3	0.7	7			
36		TH				2.6	0.4	7			
37	WW-D	TH	542837	3707106	40.28				3.2	0.6	7.5
38		NW							5.7	0.75	7
39	WW-E	TH	542765	3707142	40.36				3	0.4	6.5
40		SE							4	0.3	6.5
41	WW-12	SE	542716	3707188	40.43	5.7	0.7	6.5			
42		TH				3.3	0.6	6			
43	WW-13	TH	542500	3707442	40.75	3.2	0.4	8	3.2	0.6	7
44		BC				3.3	0.6	6	2.8	0.4	7
45		SE							3.7	0.7	6
46	WW-14	SE	541645	3708068	41.81	3.5	0.5	7	3.6	0.6	6.5
47		SE				5.4	0.7	7.5	4.8	0.5	7
48		TH							3.3	0.4	6.5
49		NW				2.2	0.6	7	2.3	0.4	7

Anza-Burnt Valley displacement data (BV)

#	Location	Feature	Longitude	Latitude	Distance along fault	Field Meters	Field ±	Field Confidence	LiDAR (QTM) Meters	LiDAR (QTM) ±	LiDAR (QTM) Confidence
1	BV-1	TH	537733	3711403	46.92	3.3	0.4	7.5	3.2	0.5	7.5
2		NW				3.5	0.3	7.5			
3	BV-A	TH	536748	3712306	48.24				3	0.3	8
4		NW							3	0.4	7
5		SE							3.2	0.3	7
6	BV-2	TH	536724	3712345	48.28	3.2	0.4	5.5			
7	BV-3	TH	536602	3712424	48.43	3.5	0.5	7.5	3.1	0.3	7
8		SE				3.4	0.4	7.5	3.2	0.4	7
9	BV-B	TH	536581	3712442	48.46				6.5	0.6	7
10		NW	536581						6.7	0.5	7
11	BV-4	TH	536541	3712464	48.5	3.7	0.3	7.75	3.4	0.5	7
12		TH				2.8	0.4	7			
13	BV-5	TH	536499	3712504	48.56	3.5	0.3	9.5	3.8	0.4	8
14		SE				3.7	0.4	9.5	3.9	0.4	8
15		NW				3.4	0.3	9.5	4	0.5	8
16	BV-6	NW	535989	3712877	49.19	3.3	0.5	7.75			
17		TH				3.6	0.6	7.75			
18		TH				5.4	0.6	6.5	5.6	0.4	7
19	BV-7	TH	535958	3712894	49.23	2.4	0.4	7			
20		TH				3.6	0.5	7.75	3.5	0.4	7
21		NW							3.2	0.3	7
22	BV-8	TH	533730	3714456	51.95	3.3	0.3	7.5	3.1	0.3	7.5
23		NW				3.2	0.4	7.5	3.4	0.4	7.5
24		SE				2.6	0.4	7.5	3.3	0.4	6.75

Anza Valley displacement data (AV)

#	Location	Feature	Longitude	Latitude	Distance along fault	Field Meters	Field ±	Field Confidence	LiDAR (QTM) Meters	LiDAR (QTM) ±	LiDAR (QTM) Confidence	LiDAR (LaDiCaoz) Meters	LiDAR (LaDiCaoz) ±	LiDAR (LaDiCaoz) Confidence
1	AV-1_17	TH	535977	3712869	49.2	3.4	0.5	10	3.6	0.5	9	3.8	0.5	8
2	AV-2_59	TH	533729	3714456	51.95	2	0.5	7.5	2.9	0.5	7	3	0.4	7
3	AV-4_57	TH	533677	3714492	52.01	0.65	0.2	5.5	1.1	0.5	4	0.9	0.4	6
4		NW				0.5	0.25	5.5						
5	AV-3_58	TH	533685	3714497	52.01	2.2	0.5	7.5	2.8	0.6	7	2.5	0.5	7
6		SE				2	0.5	6.5						
7	AV-6_53	TH	533551	3714592	52.17	0.5	0.15	5						
8	AV-5_54	TH	533561	3714599	52.17	0.55	0.2	6						
9		NW				0.55	0.2	6						
10		SE				0.4	0.1	5						
11	AV-7_55	TH	533450	3714665	52.3	2.05	0.25	8	2.2	0.6	6	2.3	0.3	5
12	AV-8_61	TH	533276	3714852	52.55	1.2	0.25	4	1.8	0.4	2			
13	AV-10_63a	NW	533216	3714861	52.6	2	0.5	5						
14	AV-10_63b	TH										11	1.5	5
15	AV-9_62	TH	533229	3714884	52.61	1	0.3	4	1.2	0.2	2			
16	AV-9_62b	TH										4	0.3	6
17	AV-11_71	RN	530474	3716834	55.99	6.6	0.5	10						
18	AV-12_70	TH	530389	3716886	56.09	3.3	0.375	9	3	0.6	4			
19		NW				3.4	0.5	9						
20		SE				3.75	0.5	8						
21	AV-13_69a	TH	530357	3716908	56.13	3.6	0.5	8.5	3.8	1	2			
22	AV-13_69b	TH							7.3	1	5			
23	AV-14_75a	RN	529970	3717166	56.6	3.9	0.5	10	4.1	0.8	7			
24	AV-14_75b	RN							20	2	7			

Horse Creek Ridge Drainage-Rouse Hill displacement data (HCRD)

#	Location	Feature	Longitude	Latitude	Distance along fault	Field Meters	Field ±	Field Confidence	LiDAR (QTM) Meters	LiDAR (QTM) ±	LiDAR (QTM) Confidence	LiDAR (LaDiCaoz) Meters	LiDAR (LaDiCaoz) ±	LiDAR (LaDiCaoz) Confidence
1	HCRD-15_1	TH	526634	3719879	60.91	3	0.7	7	3.4	1	8	3.3	0.2	4
2		NW				3.2	1	7						
3	HCRD-16_2	RN	526643	3719885	60.91			7	9.1	1.3	10			
4		SE							10	1.4	8			
5	HCRD-3	TH	526622	3719891	60.92	4.25	1	5	3.6	0.6	5	3.8	0.4	2
6	HCRD-17_4	TH	526633	3719894	60.92	1.4	0.55	5	1.2	0.5	4	1.3	0.3	2
7	HCRD-18_46	TH	526316	3720141	61.32	2.2	0.7	6	2.2	0.7	6			
8		NW				2.4	0.7	6						
9		SE				2.5	0.7	6						
10	HCRD-20_36	TH	526147	3720260	61.52	1.65	0.7	8	2.8	1.2	6			
11		SE				2	0.7	8						
12	HCRD-19_37	TH	526153	3720264	61.52	1	0.5	6.5	1.3	0.4	10			
13		NW				1	0.3	6.5						
14		SE				0.8	0.3	6.5						
15	HCRD-21_39	TH	526027	3720363	61.68	1.45	0.6	5	1.6	0.5	8			
16	HCRD-22_41	TH	525894	3720465	61.85	2	0.5	7.5	2.7	0.6	10			
17	HCRD-23_40	BC	525890	3720468	61.86	1.85	0.4	7.5	2.6	0.5	6			
18	HCRD-23.2	TH	525485	3720776	62.37				4.1	0.5	8	4	1	7
19	HCRD-23.5	TH	524475	3721426	63.57				3.9	0.7	7	4.5	0.4	10
20	HCRD-24_43	TH	523658	3721997	64.57	1.65	0.6	9.5	1.9	0.5	10	1.6	0.2	10
21	HCRD-25_45	TH	523398	3722165	64.87	9	1	7.5	9	1.5	6			
22	HCRD-26-44	TH	523409	3722197	64.88				2.5	0.5	8			
23	HCRD-26_44a	SE	523394	3722181	64.88	9.2	1	8.5	11.6	2	10			
24		TH							11.3	2	10	14.5	1	8
25	HCRD-26_44b	SE	523394	3722181	64.88	12	1	8.5						
26	HCRD-26.5	TH	522378	3723177	66.31				3.7	0.8	7	3.5	0.5	7.5
27	HCRD-26.6	TH	522226	3723278	66.49				11.5	2	7			
28	HCRD-27_79	TH	520608	3724372	68.45				5.4	1	6	6.3	1	7
29	HCRD-28_78	TH	520566	3724409	68.5	5.5	1	5.5	5	0.6	6	4.5	0.5	6
30	HCRD-29_77	TH	520541	3724432	68.53	3.3	0.7	6.5	2.6	1	5			

Blackburn Canyon displacement data (BBC)

#	Location	Feature	Longitude	Latitude	Distance along fault	Field Meters	Field ±	Field Confidence	LiDAR (QTM) Meters	LiDAR (QTM) ±	LiDAR (QTM) Confidence	LiDAR (LaDiCaoz) Meters	LiDAR (LaDiCaoz) ±	LiDAR (LaDiCaoz) Confidence
1	BBC-30_16	TH	517349	3726701	72.47	6.2	1.5	6.5	5.9	0.7	7	5.7	0.5	8
2	BBC-31_68	TH	516579	3727162	73.37	2	1	6.5	1.55	0.7	7			
3	BBC-33_66	TH	516390	3727228	73.57	1.6	1	5						
4	BBC-34_65	TH	516360	3727246	73.61	1.75	0.75	5	1.7	0.3	9	1.8	0.2	7
5	BBC-35_15a	TH	516310	3727274	73.67	1.45	0.2	10						
6		NW				1.3	0.4	10						
7		SE				1.2	0.35	10						
8	BBC-35_15b	TH	516310	3727274	73.67	3	1	8	2.9	0.4	8			
9	BBC-36_64	TH	516288	3727287	73.69	3.8	1	5	3.2	0.3	4	4	0.8	5
10		NW				3.8	1	5						
11		SE				3.8	1	5						
12	BBC-37_6	TH	516154	3727384	73.85	1.1	0.4	7.5	1.3	0.5	2			
13		SE			73.85	1.15	0.5	7.5						
14	BBC-38_8	TH	516149	3727388	73.86	1.15	0.4	6.5						
15		NW				1.2	0.4	6.5						
16		SE				1.2	0.5	6.5						
17	BBC-39_5	TH	516142	3727393	73.87	1.15	0.3	8						
18	BBC-40_7	TH	516122	3727407	73.9	1.1	0.45	4						
19	BBC-41_10	RN	516069	3727433	73.95	3.1	0.5	10						
20		TH				2.9	1	9.5						
21	BBC-42_11	RN	516063	3727436	73.96	0.95	0.2	10						
22	BBC-43_12	TH	516026	3727462	74.01	0.9	0.4	6						
23		SE				1.2	0.7	6						
24	BBC-44_12.5	TH	516000	3727477	74.04	7.4	1.5	6	7.5	1	10	7.6	0.5	10
25	BBC-45_14	TH	515916	3727548	74.15	4	1	9	2.6	0.3	2			
26		NW				3.85	0.6	9						
27		SE				3.7	0.6	9						
28	BBC-46_32	TH	515562	3727772	74.56	0.9	0.4	7						
29	BBC-47_31	TH	515463	3727844	74.69	1.6	0.4	7.5	2.1	0.3	8	2	0.5	6
30	BBC-48_30	TH	515433	3727868	74.73	0.95	0.4	7	0.9	0.4	5			
31		SE				0.7	0.4	7						
32	BBC-49_29	TH	515371	3727900	74.8	0.75	0.3	5	0.7	0.2	5			
33	BBC-50_27	TH	515169	3728005	75.02	0.6	0.3	7						
34	BBC-51_26	TH	515167	3728006	75.03	0.7	0.4	6						
35	BBC-52_25	TH	515162	3728008	75.03	0.5	0.3	6.5						
36	BBC-53_23	TH	514923	3728074	75.27	1.55	0.5	6						
37		SE				1.35	0.5	6						
38	BBC-54_22	TH	514817	3728150	75.4	1.7	0.4	7						

Figure Captions

Figure 1. Location of the Clark strand (bolded) of the San Jacinto fault zone relative to the southern San Andreas fault system, highlighting significant earthquakes since 1899 (modified from Rockwell et al., 2000).

Figure 2. Detailed geologic map of the Clark fault (simplified from Sharp, 1967). The study area is separated into nine sections, bounded by areas where offsets are not preserved or are buried. Within these nine sections we estimated displacement on channel margins, thalwegs, rills, and ridge noses. Abbreviated geologic units: Qal - Quaternary alluvium, Qt - Quaternary terrace sands and gravels, Qb - Quaternary Bautista beds, KTc - Cretaceous and Tertiary augen gneisses and mylonites, Kga – mid-Cretaceous medium to coarse-grained garnetiferous adamellites, Kmg – mid-Cretaceous medium-grained granodioritic rocks, Ka – mid-Cretaceous medium-grained adamellitic rocks, Ktg – mid-Cretaceous fine to medium-grained tonalites and granodiorites, Kfa – mid-Cretaceous fine to medium-grained biotite adamellite, Kt – mid-Cretaceous tonalitic rocks, Kdg – inequigranular granodiorites and adamellites, Kg – mid-Cretaceous norites, gabbros, and leucogabbros, pKm – pre mid-Cretaceous banded gneisses.

Figure 3. (a) Field and LiDAR-based displacement measurements made along the Clark fault from the western Salton Trough (km 0) to the San Jacinto Valley (km 80). Abbreviated study area subdivisions, from km 0 – 80: LR – Lute Ridge, RR/RC – Rockhouse Ridge and Rockhouse Canyon, JAR – Jackass Ridge, DW – Dry Wash, HC/WW – Horse Canyon and White Wash, AV/BV – Anza Valley and Burnt Valley, HCRD/RH – Horse Creek Ridge Drainage and Rouse Hill, BBC – Blackburn Canyon. (b) Cumulative stack of displacement measurements weighted by assigned quality estimates (0-5 = Poor, 5.25-6.75 = Fair, 7-8.75= Good, and 9-10 = Excellent)

Figure 4. (a) Graph displaying estimated displacement from fieldwork and high resolution B4 LiDAR DEM's along Lute Ridge. (b) Cumulative stack of displacement measurements weighted by assigned quality estimates (0-5 = Poor, 5.25-6.75 = Fair, 7-8.75= Good, and 9-10 = Excellent)

Figure 5. (a) Graph displaying estimated displacement from fieldwork and high resolution B4 LiDAR DEM's along Rockhouse Ridge and through Rockhouse Canyon. (b) Cumulative stack of displacement measurements weighted by assigned quality estimates (0-5 = Poor, 5.25-6.75 = Fair, 7-8.75= Good, and 9-10 = Excellent)

Figure 6. (a) Graph displaying estimated displacement from fieldwork and high resolution B4 LiDAR DEM's along Jackass Ridge. (b) Cumulative stack

of displacement measurements weighted by assigned quality estimates (0-5 = Poor, 5.25-6.75 = Fair, 7-8.75= Good, and 9-10 = Excellent)

Figure 7. (a) Graph displaying estimated displacement from fieldwork and high resolution B4 LiDAR DEM's through Dry Wash. (b) Cumulative stack of displacement measurements weighted by assigned quality estimates (0-5 = Poor, 5.25-6.75 = Fair, 7-8.75= Good, and 9-10 = Excellent)

Figure 8. (a) Graph displaying estimated displacement from fieldwork and high resolution B4 LiDAR DEM's through Horse Canyon and White Wash. (b) Cumulative stack of displacement measurements weighted by assigned quality estimates (0-5 = Poor, 5.25-6.75 = Fair, 7-8.75= Good, and 9-10 = Excellent)

Figure 9. (a) Graph displaying estimated displacement from fieldwork and high resolution B4 LiDAR DEM's through Anza Valley and Burnt Valley. (b) Cumulative stack of displacement measurements weighted by assigned quality estimates (0-5 = Poor, 5.25-6.75 = Fair, 7-8.75= Good, and 9-10 = Excellent)

Figure 10. (a) Graph displaying estimated displacement from fieldwork and high resolution B4 LiDAR DEM's through Horse Creek Ridge Drainage and along Rouse Hill. (b) Cumulative stack of displacement measurements weighted by assigned quality estimates (0-5 = Poor, 5.25-6.75 = Fair, 7-8.75= Good, and 9-10 = Excellent)

Figure 11. (a) Graph displaying estimated displacement from fieldwork and high resolution B4 LiDAR DEM's through Blackburn Canyon. (b) Cumulative stack of displacement measurements weighted by assigned quality estimates (0-5 = Poor, 5.25-6.75 = Fair, 7-8.75= Good, and 9-10 = Excellent)

Figure 12. Comparison of measurements made across different apertures along strike. Where field and LiDAR measurements exist for a single feature, the LiDAR measurement value was subtracted from the field measurement value. Positive values indicate field measurements that are larger than LiDAR measurements and negative values indicate LiDAR measurements that are larger than field measurements.

Figure 13. Comparison of the measurement discrepancy (in meters) across apertures vs. the quantity of offsets with said measurement discrepancy.

Figure 14. Scenario A - Slip distribution graph for the most recent events on the Clark fault. Data points represent the most reliable and best-preserved features (good and excellent) to estimate displacement. We attribute the 3-4 m offsets through the Anza region to the most recent, large-scale rupture event on the Clark fault. We also recognize the likely rupture from the 21 April 1918 earthquake, which broke a short ~15-20 km section of the fault (with an average of 1.25 m of right-lateral

displacement) in Blackburn Canyon, apparently due to lower displacement in that area in the ca. 1800 event.

Figure 15. Scenario B - Slip distribution graph for the most recent events on the Clark fault. Data points represent the most reliable and best-preserved features to estimate displacement. We attribute all mapped offsets less than 4 m (including the 0.5-1.75 m offsets in Blackburn Canyon) to a single large rupture event. The rapid die-off of displacement to the northwest suggests that the rupture may have terminated at the northwest end of Blackburn Canyon, thereby totaling just over ~75 km in length. We do not prefer this interpretation because there appear to be two ages of displacements in this cluster, with the smaller offsets appearing fresher and younger than the larger ones.

Figure 16. Isoseismal maps of earthquake events, modified from Toppozada et al., 1981. (A) February 9th, 1890, (B) May 28th, 1892, (C) December 25th, 1899, (D) April 21st, 1918, (E) November 22nd, 1800, assuming MMI VII values at San Juan Capistrano and San Diego missions, (F) November 22nd, 1800, assuming MMI VI-VI+ values at San Juan Capistrano and San Diego missions. Abbreviated California city names: S.L.O. – San Luis Obispo, S.B. – Santa Barbara, V. – Ventura, L.A. – Los Angeles, S.J.C. – San Juan Capistrano, S.D. – San Diego, Y. – Yuma, N. – Needles.

Online Material

Appendix, containing annotated topographic contour maps and hillshades derived from raw and filtered B4 LiDAR data, corresponding field photographs, and data tables comparing LiDAR-based and field-based slip measurements for individual geomorphic features along the Clark fault.

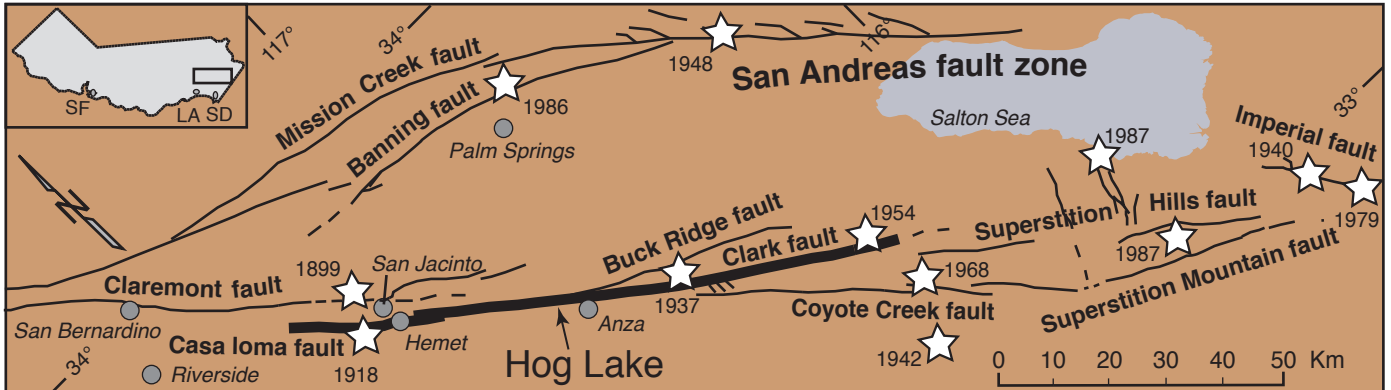
SF
LA SD
117°
34°
116°
33°
Mission Creek fault
Banning fault
1986
Palm Springs
1948
San Andreas fault zone
Salton Sea
1987
Imperial fault
1940
1979
Hills fault
1987
Superstition
Superstition Mountain fault
1954
Buck Ridge fault
Clark fault
1968
Coyote Creek fault
1942
1937
Anza
Hog Lake
Claremont fault
1899
San Jacinto
San Bernardino
Casa loma fault
1918
Hemet
Riverside
0 10 20 30 40 50 Km

Figure 1

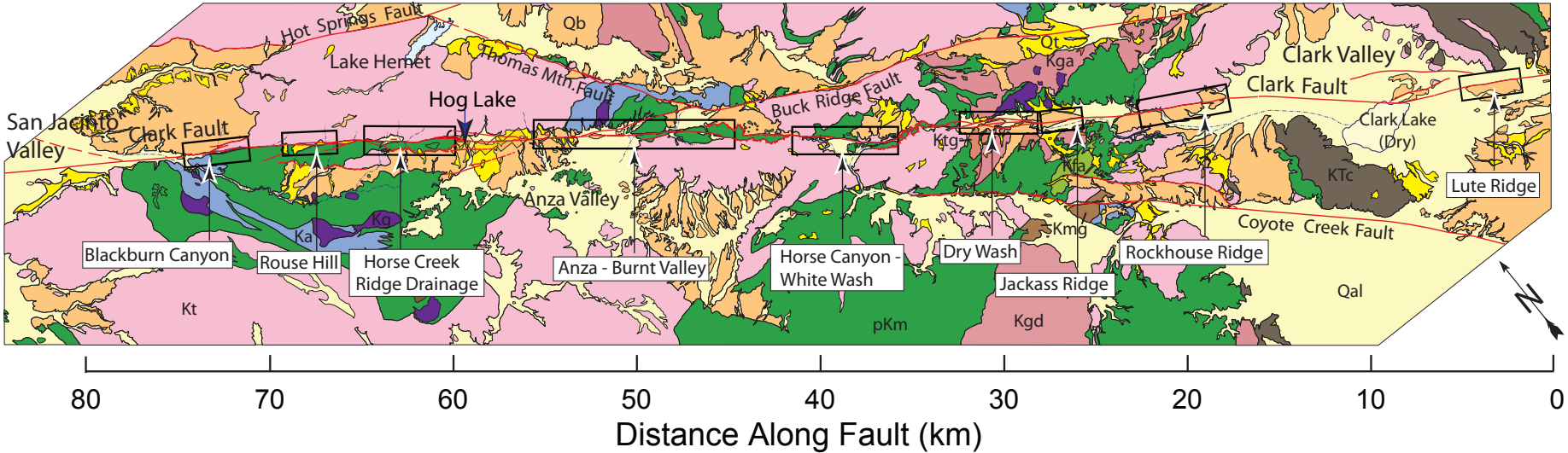
Hot Springs Fault
Qb
Lake Hemet
Thomas Mtn. Fault
Hog Lake
Buck Ridge Fault
Qt
Kga
Clark Valley
Clark Fault
San Jacinto Valley
Clark Fault
Clark Lake (Dry)
Ktg
Kfa
KTc
Lute Ridge
Anza Valley
Kg
Ka
Kmg
Coyote Creek Fault
Blackburn Canyon
Rouse Hill
Horse Creek Ridge Drainage
Anza - Burnt Valley
Horse Canyon - White Wash
Dry Wash
Rockhouse Ridge
Jackass Ridge
Kt
pKm
Kgd
Qal
N
80
70
60
50
40
30
20
10
0
Distance Along Fault (km)

Figure 2

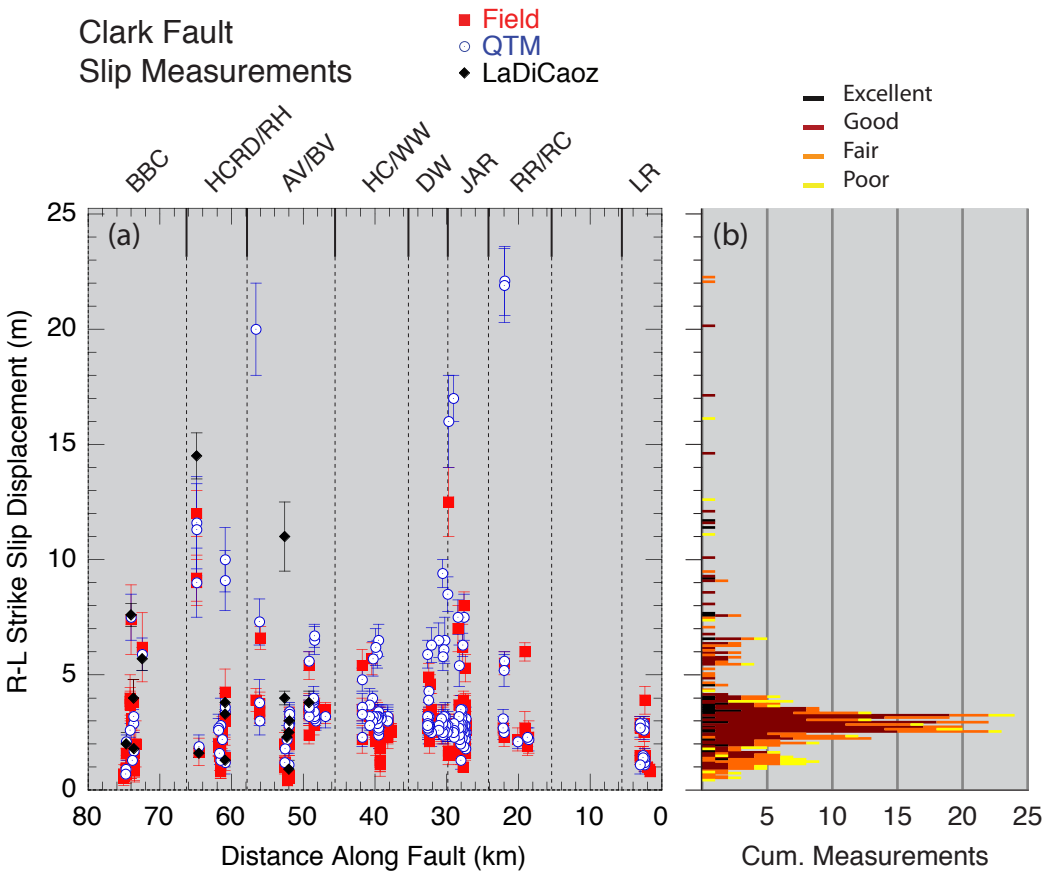
Clark Fault
Slip Measurements
Field
QTM
LaDiCaoz
Excellent
Good
Fair
Poor
BBC
HCRD/RH
AV/BV
HC/WW
DW
JAR
RR/RC
LR
(a)
(b)
R-L Strike Slip Displacement (m)
Distance Along Fault (km)
Cum. Measurements
0
5
10
15
20
25
80
70
60
50
40
30
20
10
0

Figure 3

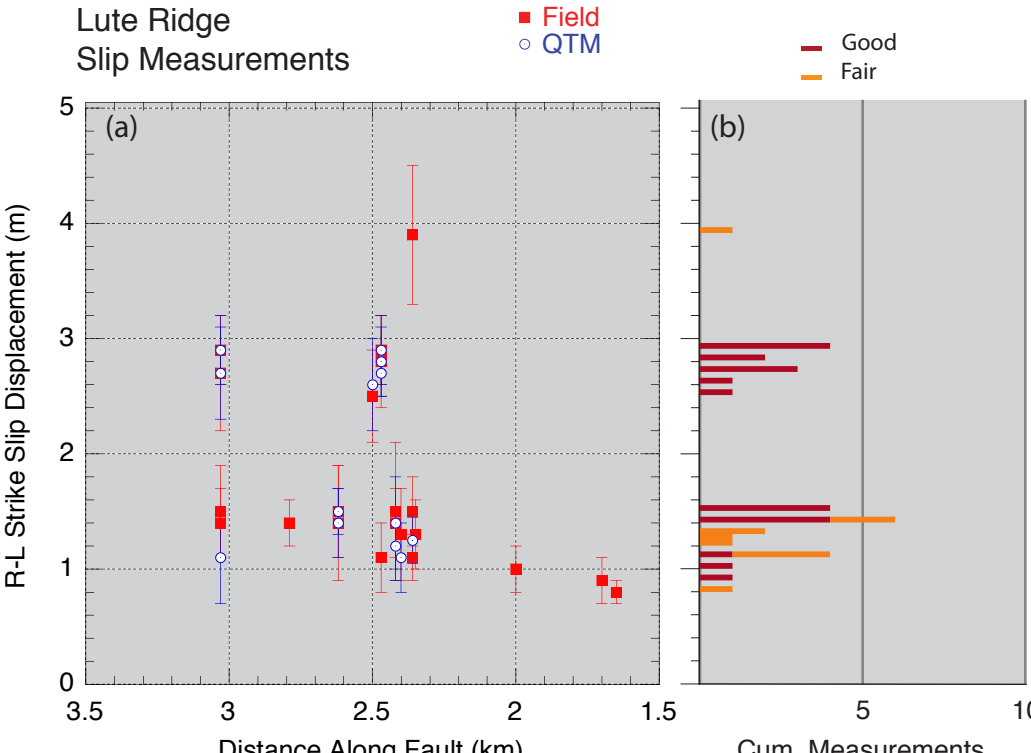
Lute Ridge
Slip Measurements
Field
QTM
Good
Fair
(a)
(b)
R-L Strike Slip Displacement (m)
0
1
2
3
4
5
3.5
3
2.5
2
1.5
Distance Along Fault (km)
5
10
Cum. Measurements

Figure 4

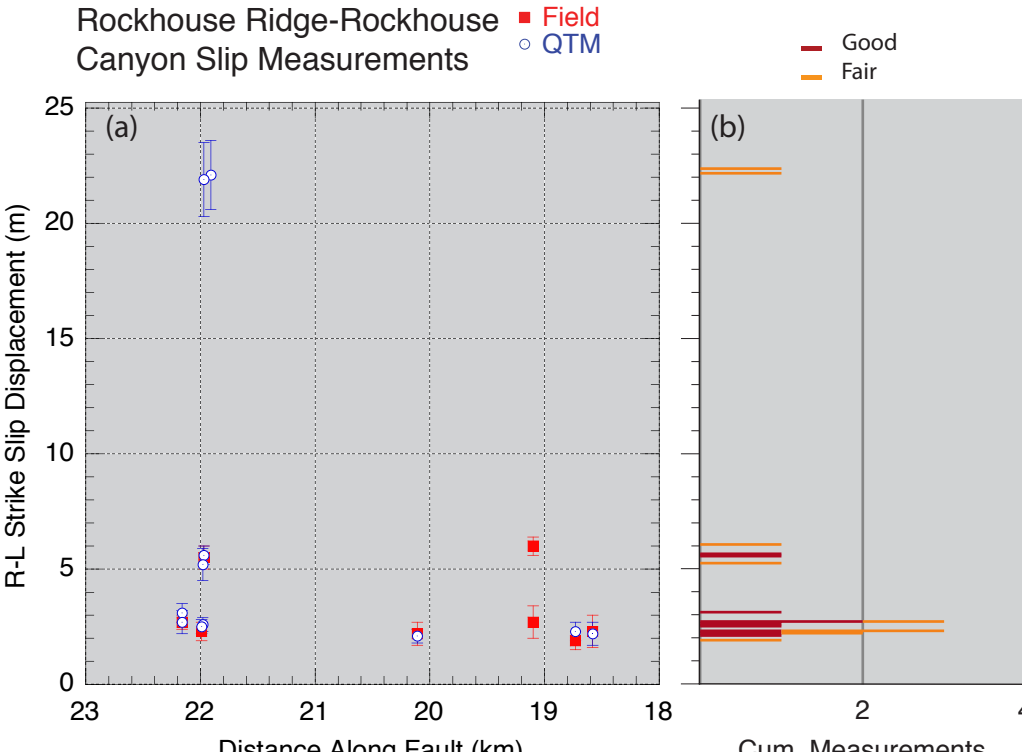
Rockhouse Ridge-Rockhouse Canyon Slip Measurements
Field
QTM
Good
Fair
(a)
(b)
R-L Strike Slip Displacement (m)
25
20
15
10
5
0
23
22
21
20
19
18
Distance Along Fault (km)
2
4
Cum. Measurements

Figure 5

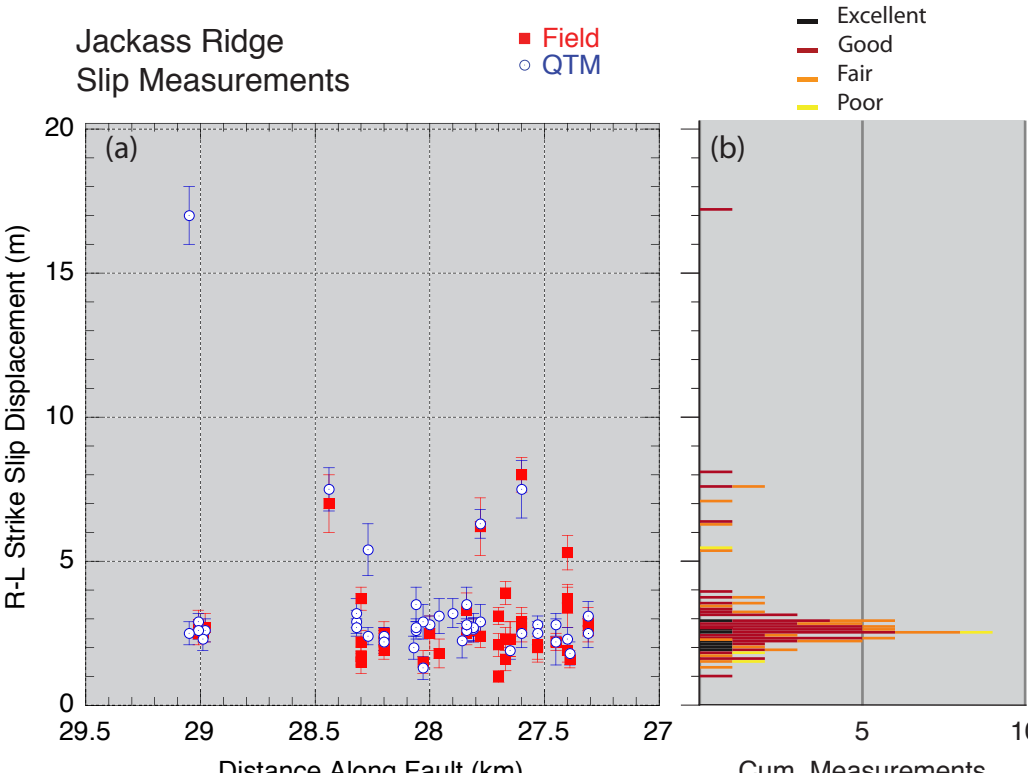
Jackass Ridge
Slip Measurements
Field
QTM
Excellent
Good
Fair
Poor
(a)
(b)
R-L Strike Slip Displacement (m)
20
15
10
5
0
29.5
29
28.5
28
27.5
27
Distance Along Fault (km)
5
10
Cum. Measurements

Figure 6

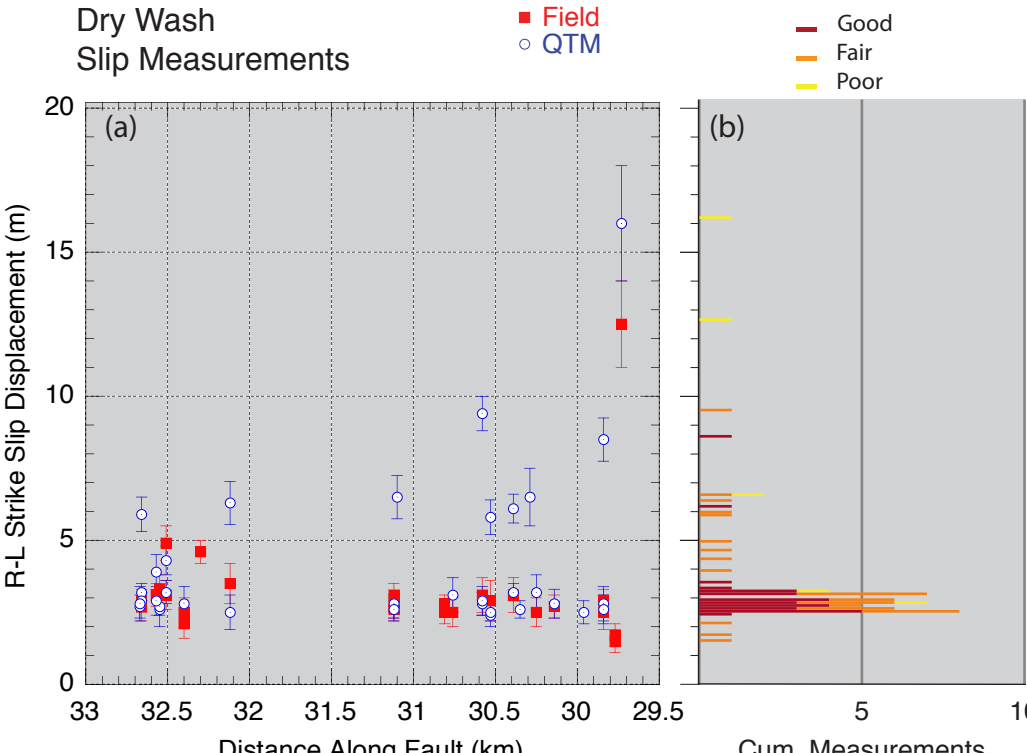
Dry Wash
Slip Measurements
Field
QTM
Good
Fair
Poor
(a)
(b)
R-L Strike Slip Displacement (m)
20
15
10
5
0
33
32.5
32
31.5
31
30.5
30
29.5
Distance Along Fault (km)
5
10
Cum. Measurements

Figure 7

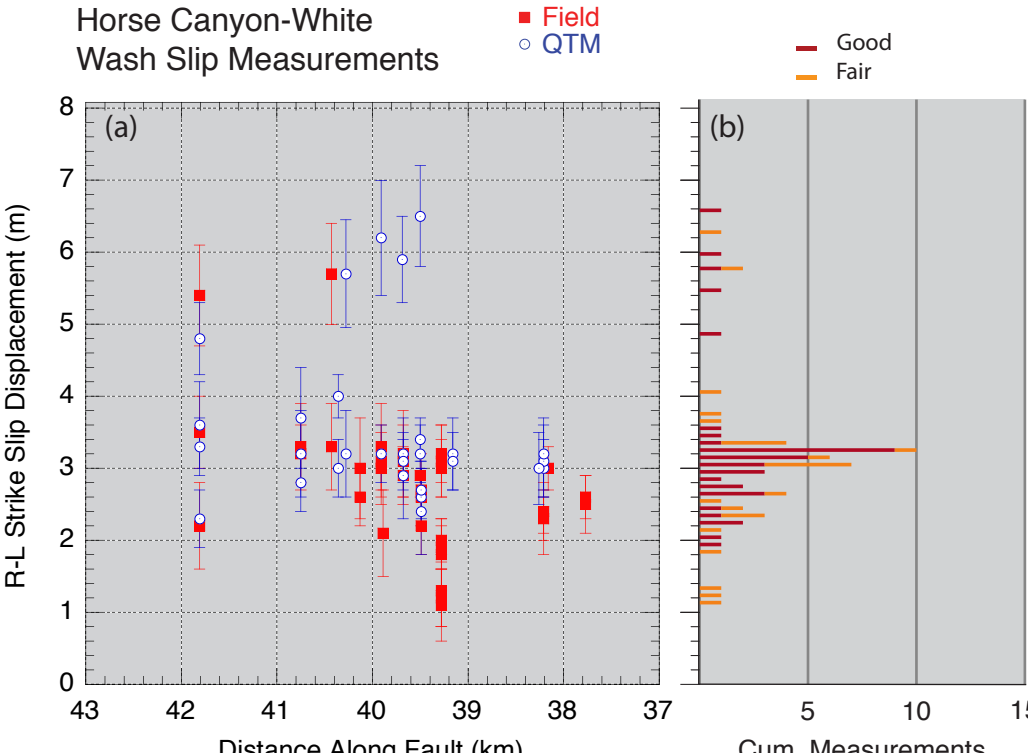
Horse Canyon-White
Wash Slip Measurements
Field
QTM
Good
Fair
(a)
(b)
R-L Strike Slip Displacement (m)
0
1
2
3
4
5
6
7
8
43
42
41
40
39
38
37
Distance Along Fault (km)
5
10
15
Cum. Measurements

Figure 8

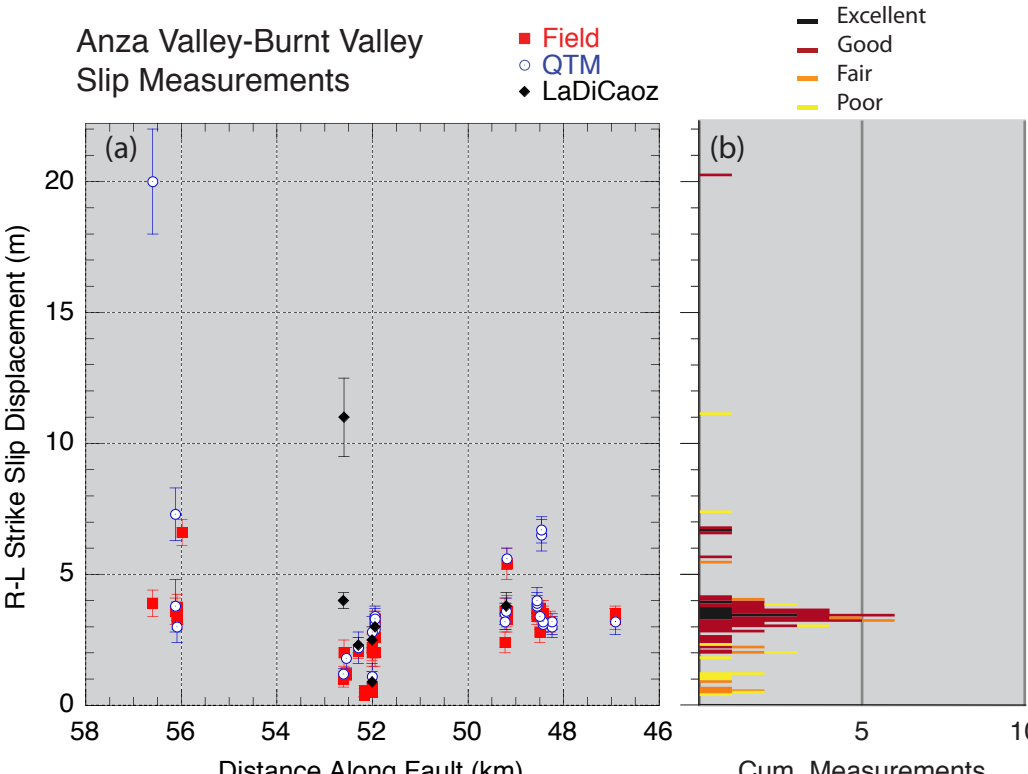
Anza Valley-Burnt Valley
Slip Measurements
Field
QTM
LaDiCaoz
Excellent
Good
Fair
Poor
(a)
(b)
R-L Strike Slip Displacement (m)
0
5
10
15
20
58
56
54
52
50
48
46
Distance Along Fault (km)
5
10
Cum. Measurements

Figure 9

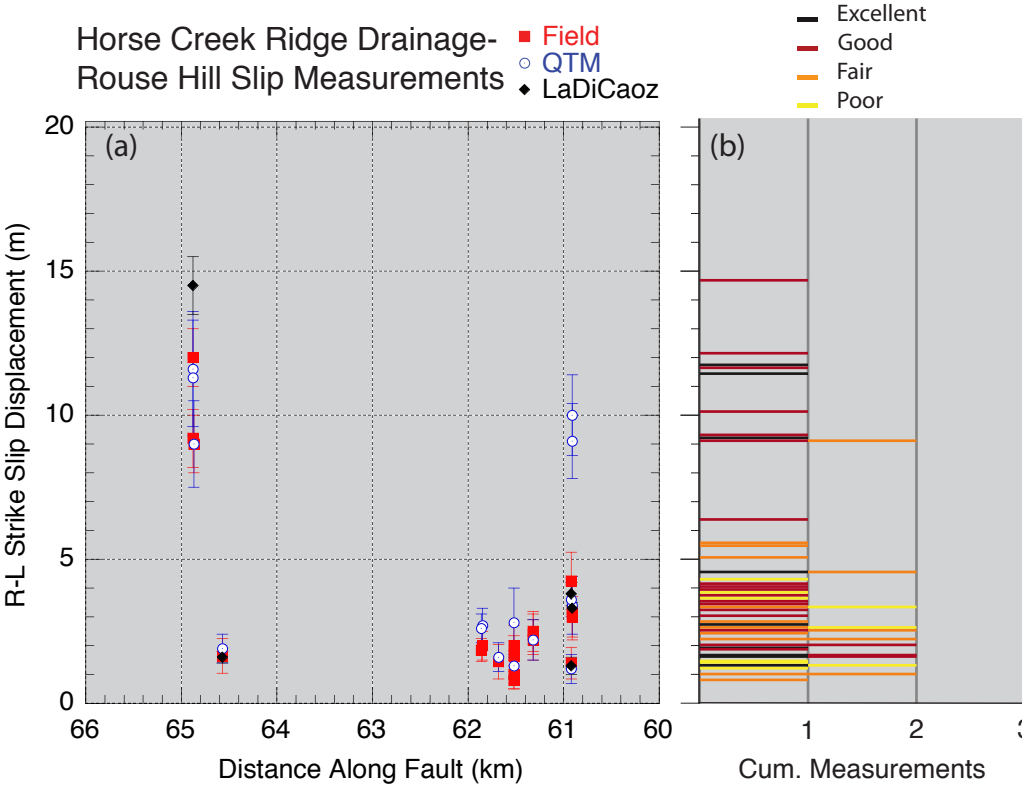
Horse Creek Ridge Drainage-
Rouse Hill Slip Measurements
Field
QTM
LaDiCaoz
Excellent
Good
Fair
Poor
(a)
(b)
R-L Strike Slip Displacement (m)
20
15
10
5
0
66
65
64
63
62
61
60
Distance Along Fault (km)
1
2
3
Cum. Measurements

Figure 10

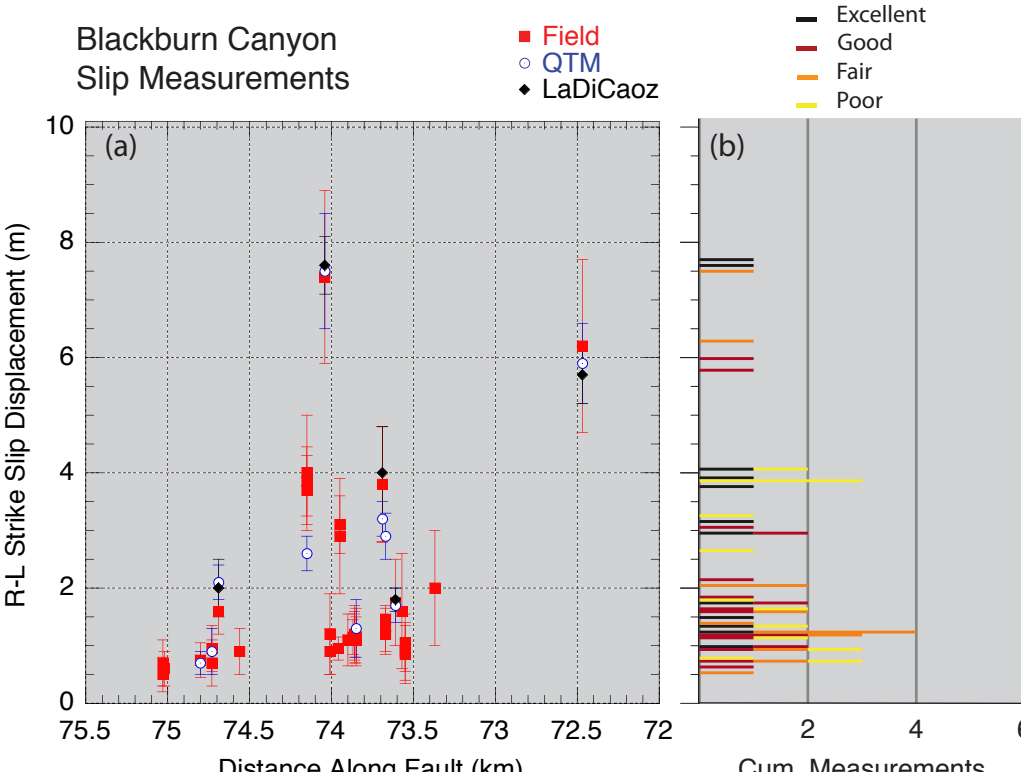
Blackburn Canyon
Slip Measurements
Field
QTM
LaDiCaoz
Excellent
Good
Fair
Poor
(a)
(b)
R-L Strike Slip Displacement (m)
0
2
4
6
8
10
75.5
75
74.5
74
73.5
73
72.5
72
Distance Along Fault (km)
2
4
6
Cum. Measurements

Figure 11

Field vs. LiDAR Measurements

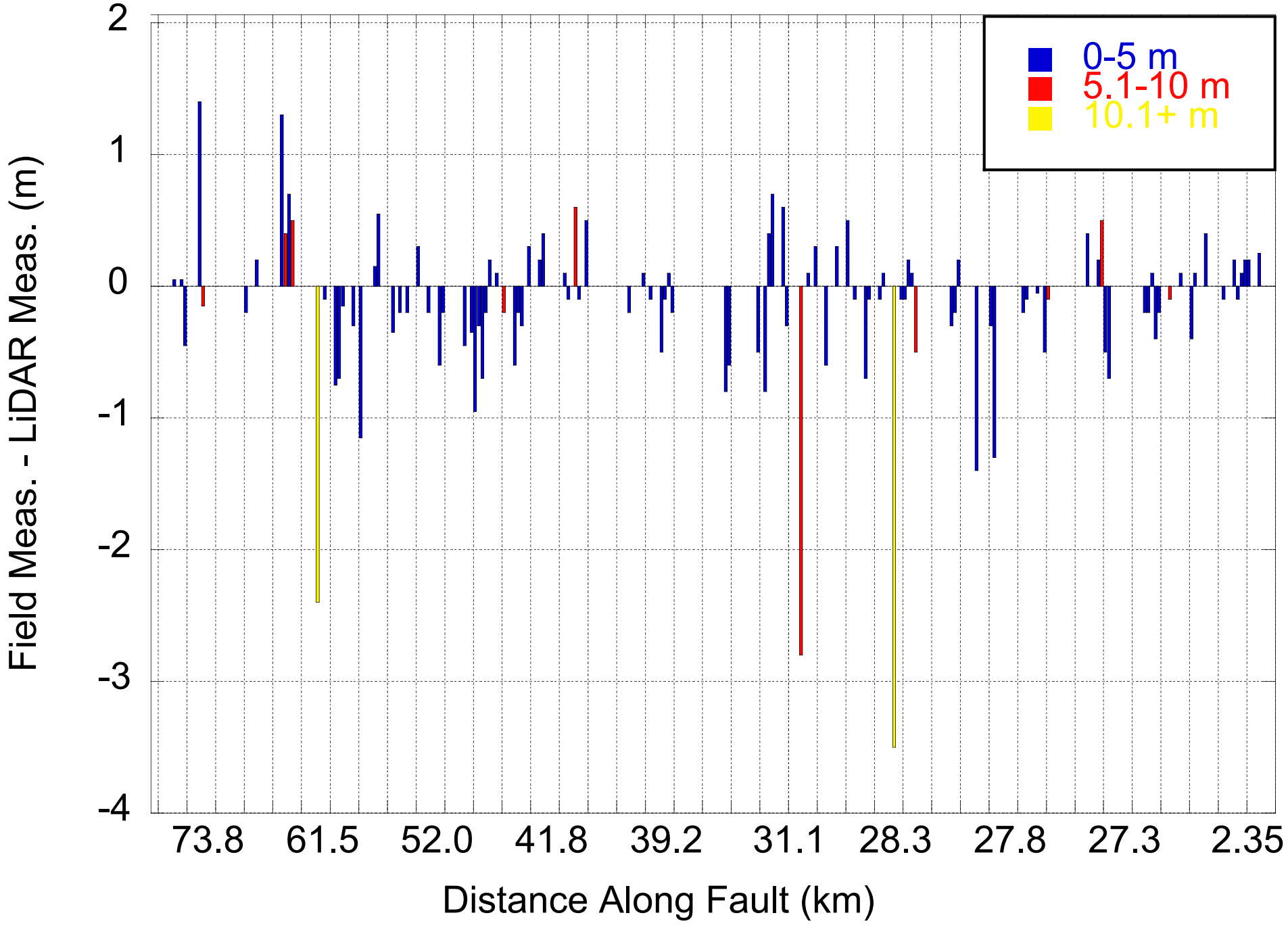

Figure 12

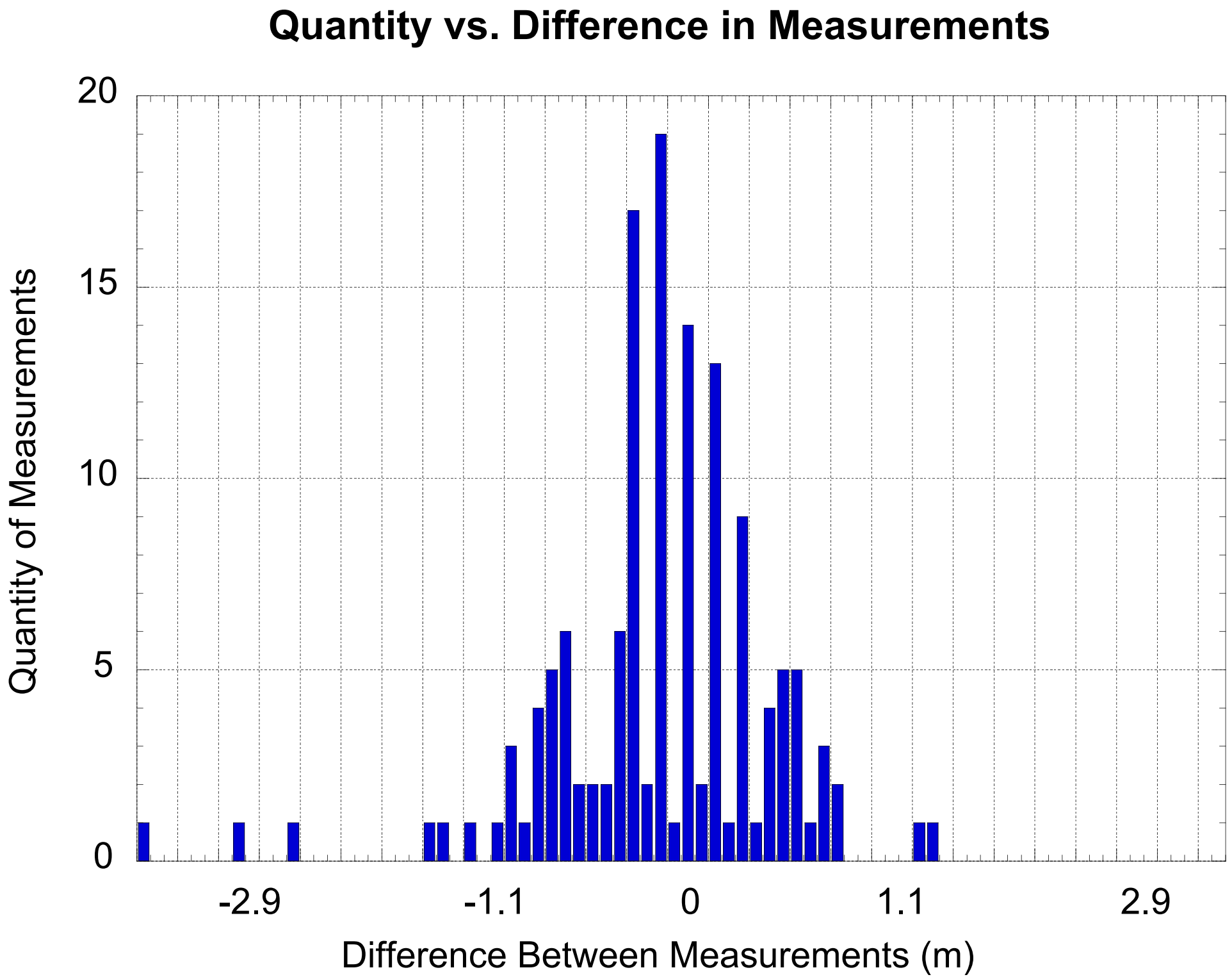
Quantity vs. Difference in Measurements
Quantity of Measurements
20
15
10
5
0
-2.9
-1.1
0
1.1
2.9
Difference Between Measurements (m)

Figure 13

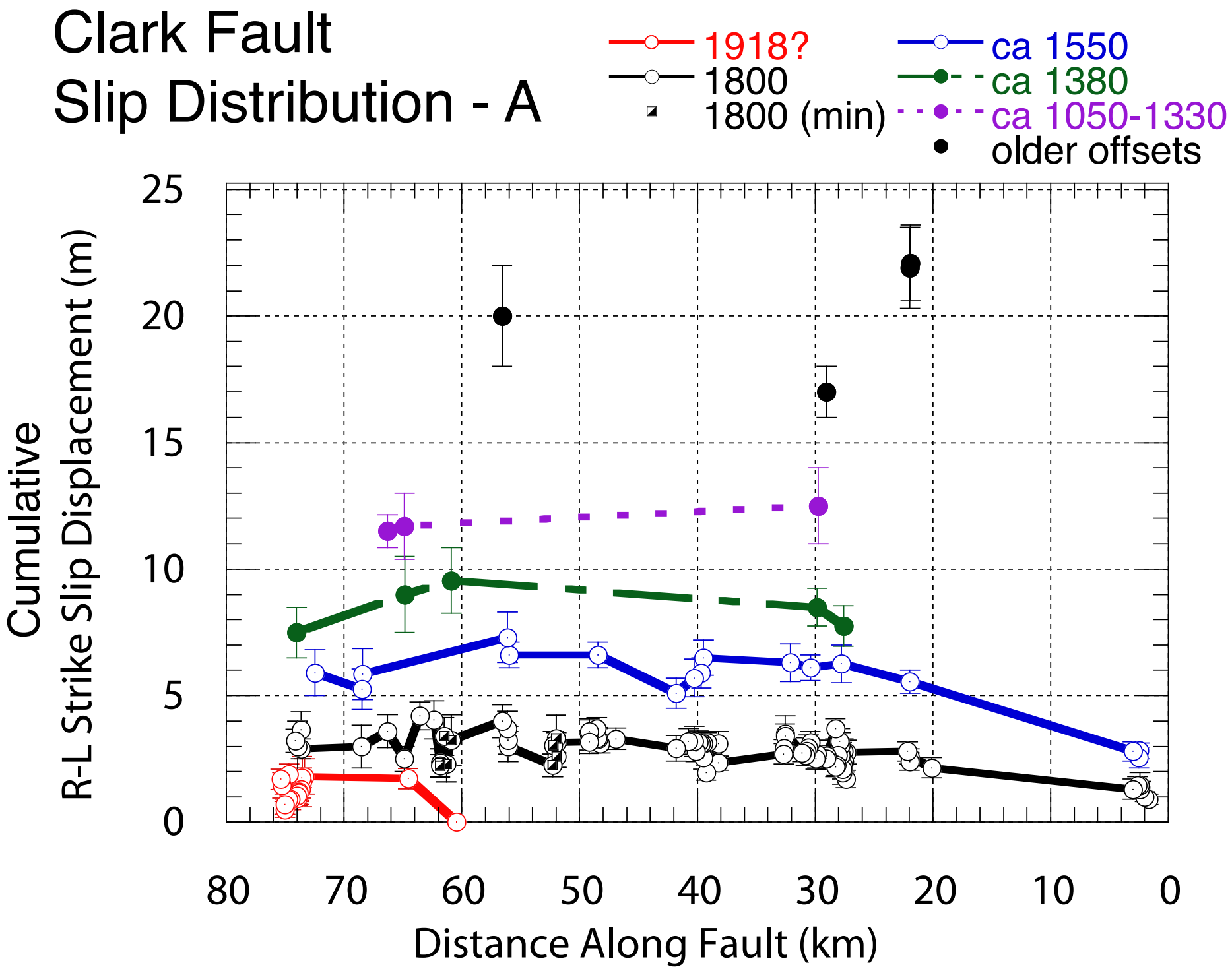
Clark Fault
Slip Distribution - A
1918?
1800
1800 (min)
ca 1550
ca 1380
ca 1050-1330
older offsets
Cumulative
R-L Strike Slip Displacement (m)
25
20
15
10
5
0
80
70
60
50
40
30
20
10
0
Distance Along Fault (km)

Figure 14

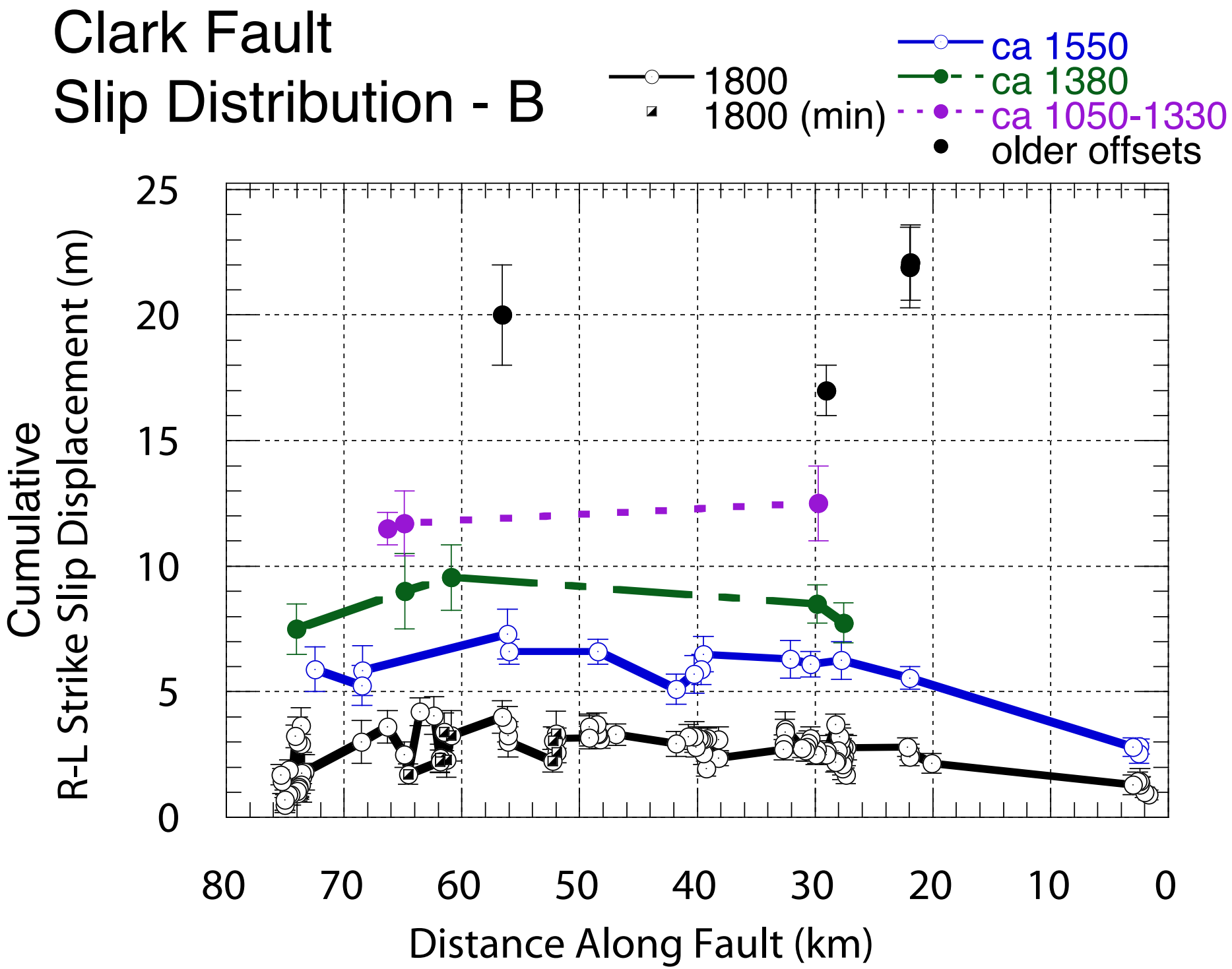
Clark Fault
Slip Distribution - B
1800
1800 (min)
ca 1550
ca 1380
ca 1050-1330
older offsets
Cumulative
R-L Strike Slip Displacement (m)
25
20
15
10
5
0
80
70
60
50
40
30
20
10
0
Distance Along Fault (km)

Figure 15

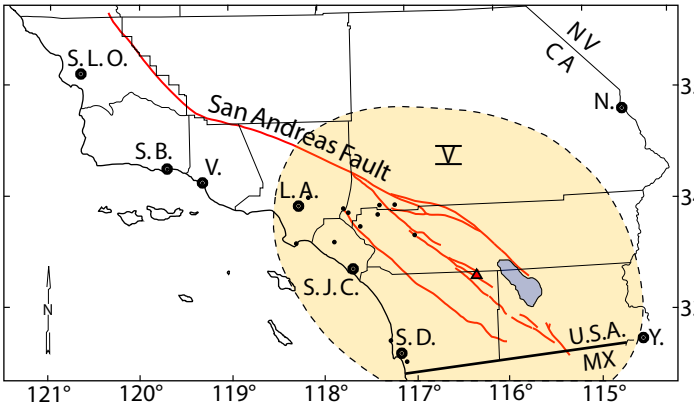

A. February 9th, 1890 - Mw<6.5

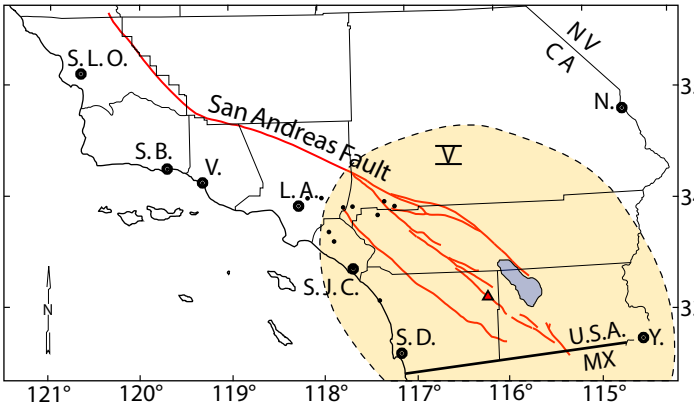

B. May 28th, 1892 - Mw<6.5

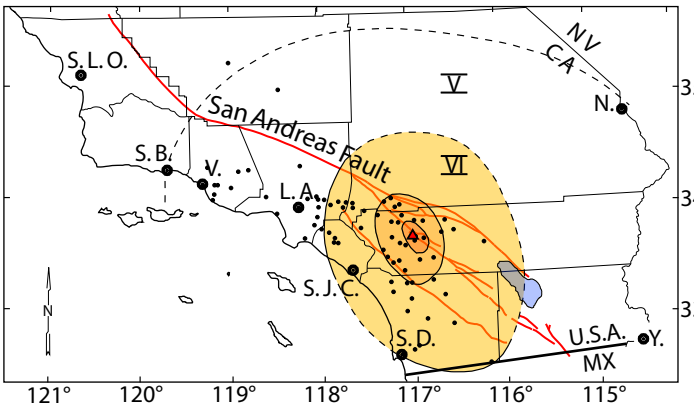

C. December 25th, 1899 - M=6.4

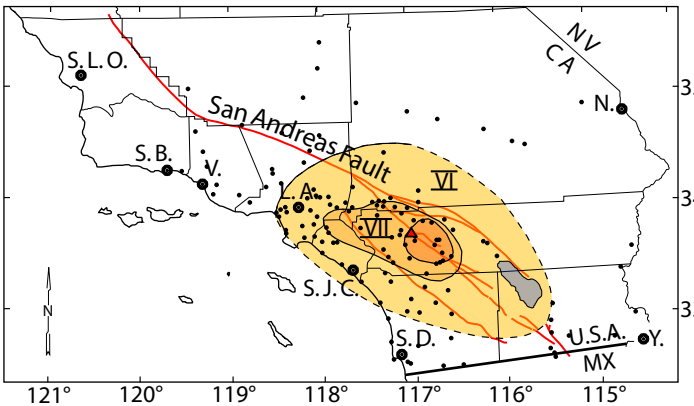

D. April 21st, 1918 - M=6.9

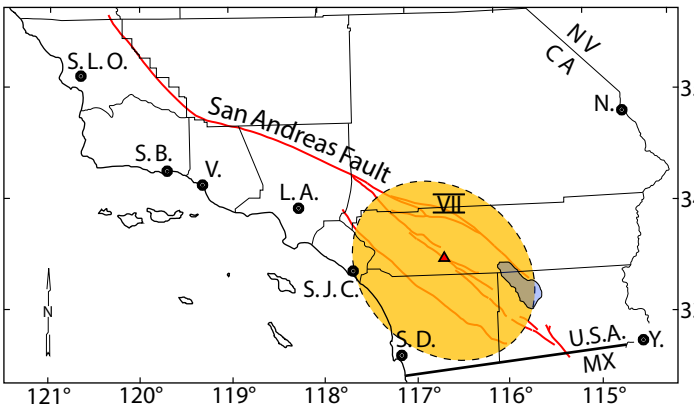

E. November 22nd, 1800 - Mw=7.8

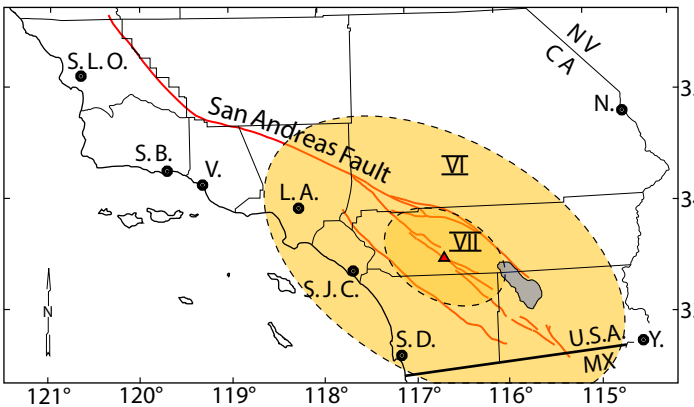

F. November 22nd, 1800 - Mw=7.2-7.6

Figure 16

Supplemental Material: Online Appendix

Click here to download Supplemental Material: Salisbury_et_al_Appendix(sm).pdf

Copyright Form
Click here to download Copyright Form_CopyrightBSSA(JB's).pdf

Bulletin of the Seismological Society of America

COPYRIGHT/PAGE-CHARGES FORM

PLEASE FILL OUT AND SUBMIT THIS FORM ONLINE WHEN SUBMITTING YOUR PAPER OR FAX IT TO FAX NUMBER 503 405 7190

Manuscript Number: BSSA-D- _____ [leave blank for new submissions]

Title: LiDAR and Field Observations of Slip Distribution for the Most Recent Surface Ruptures Along the Central San Jacinto Fault

Authors: J. B. Salisbury, Rockwell, T. K., Middleton, T. J., Hudnut, K. W.

COPYRIGHT

In accordance with Public Law 94-533, copyright to the article listed above is hereby transferred to the Seismological Society of America (for U.S. Government employees, to the extent transferable) effective if and when the article is accepted for publication in the *Bulletin of the Seismological Society of America*. The authors reserve the right to use all or part of the article in future works of their own. In addition, the authors affirm that the article has not been copyrighted and that it is not being submitted for publication elsewhere.

To be signed by at least one of the authors (who agrees to inform the others, if any) or, in the case of "work made for hire," by the employer.

Authorized Signature for Copyright	Print Name (and title, if not author)	Date
	James Barrett Salisbury	March 1, 2011

PUBLICATION CHARGES

The Seismological Society of America requests that institutions supporting research share in the cost of publicizing the results of that research. The Editor has the discretion of waiving page charges for authors who do not have institutional support. Current rates are available at http://www.seismosoc.org/publications/bssa/authors/bssa-page-charges.php

Color options: Color figures can be published in (1) color both in the online journal and in the printed journal, or (2) color online and gray scale in print. Online color is free; authors will be charged for color in print. You must choose one option for all of the color figures within a paper; that is, you cannot choose option (1) for one color figure and option (2) for another color figure. You cannot submit two versions of the same figure, one for color and one for gray scale. You are responsible for ensuring that color figures are understandable when converted to gray scale, and that text references and captions are appropriate for both online and print versions. **Color figures must be submitted before the paper is accepted for publication. If color figures are changed to gray scale after acceptance of the paper, there will be a delay to publication while the paper undergoes further review by the Editorial Board.**
Art guidelines are at http://www.seismosoc.org/publications/bssa/authors/bssa-art-submissions.php

Will page charges be paid? Check one:

X **BOTH PAGE CHARGES AND COLOR CHARGES WILL BE PAID**, and all color figures for this paper will be color both online and in print. This option requires full payment of page and color charges. ***Before choosing this option, please ensure that there is funding to support color in print.*** **See http://www.seismosoc.org/publications/bssa/authors/bssa-page-charges.php for current rates.**

____ **ONLY PAGE CHARGES WILL BE PAID**, and all figures for this paper will be gray scale in print. Color figures, if any, will be color online.

____ **A WAIVER OF PAGE CHARGES IS REQUESTED,** and all figures will be gray scale in print. Color figures, if any, will be color online.

Send Invoice To: Dr. Thomas Rockwell, San Diego State University
Department of Geological Sciences, MC 1020
5500 Campanile Drive, San Diego, CA 92182

If your paper is accepted for publication, SSA requires that you fill out and submit an online billing/offprint form.

Questions regarding billing should be directed to the SSA Business Office,
Suite 201, Plaza Professional Building, El Cerrito, CA 94530 USA Phone 510 525-5474 Fax 510 525-7204